Int J Earth Sci (Geol Rundsch) (2006) 95: 204–224
DOI 10.1007/s00531-005-0033-y

ORIGINAL PAPER

Y. Senglaub · R. Littke · M. R. Brix

Numerical modelling of burial and temperature history as an approach for an alternative interpretation of the Bramsche anomaly, Lower Saxony Basin

Received: 11 March 2004 / Accepted: 10 September 2004 / Published online: 15 September 2005

Abstract The Lower Saxony Basin, Germany, is one of the several sedimentary basins within the Central European Basin system. In its southwestern part, anomalously high maturity of organic matter has been observed to reach 4.5% VRr in Upper Jurassic and Lower Cretaceous sedimentary rocks in an area which coincides with a magnetic and a positive gravimetric anomaly. This anomaly was often interpreted as the consequence of a deep-seated igneous intrusion, the so-called Bramsche Massif. However, results obtained from calibrated numerical modelling are not in accordance with this scenario. Instead, a burial by approximately 4 km of now-eroded Cretaceous rocks was revealed to be the probable cause for the anomaly. Data and modelling results from six boreholes and two pseudo-wells support this view.

Keywords Lower Saxony Basin · Bramsche Massif · Vitrinite reflectance · Basin modelling · Temperature history

Introduction

The Lower Saxony Basin (LSB) is one of the several sedimentary basins within the European Basin System (Ziegler 1982, 1990; van Wees et al. 2000). In its southwestern part, that is, in the area of Bramsche, evidence for extremely high thermal maturity of coaly organic matter has been found during the past decades (Teichmüller and Teichmüller 1951; Bartenstein et al. 1971; Koch and Arnemann 1975; Teichmüller et al. 1984). The central part of the anomaly is characterized by anthracitization of coal in lowermost Cretaceous sedimentary rocks (Wealden), whereas in the peripheral area coalification in the same stratigraphic level does not exceed the lignite stage (Teichmüller and Teichmüller 1958). In the centre of the anomaly, vitrinite reflectance measured on organic material from Upper Jurassic sedimentary rocks reaches values between 2.99 and 4.56% VRr, that is, the meta-anthracite rank (Bartenstein et al. 1971). Furthermore, rank gradients in the coal-bearing Carboniferous sequence are up to 0.16% in this area (Teichmüller 1963; Buntebarth 1985), whereas they are lower than 0.10% in the buried Rhenish Massif in the south (Münsterland Swell, Teichmüller et al. 1983).

Based on the above-mentioned findings and due to the presence of a magnetic (Schmidt 1914, cited in Breyer 1971) and positive gravimetric anomaly (Kaiser 1930, cited in Flotow et al. 1931; Hahn and Kind 1971), it was assumed that a deep-lying igneous intrusion, the Bramsche Massif, at more than 5 km depth heated the overlying sedimentary rocks leading to high coalification values (Mundry 1971; Thyssen et al. 1971; Buntebarth and Teichmüller 1979; Giebeler-Degro 1986). In accordance with the lignite/subbituminous coal stage of Upper Campanian rocks overlying the Lower Cretaceous units, it was concluded that the intrusion was emplaced either in late Early Cretaceous or in early Late Cretaceous times (Stadler and Teichmüller 1971). Calculations for the Ibbenbüren area by Buntebarth (1985) based on an empirical method suggested high 'geothermal gradients' for the upper crust ranging between 65 and 92°C/km which would correspond to extremely high heat flows between 140 and 175 mW/m^2 at the time of maximum burial, that is, the late Early Cretaceous or early Late Cretaceous.

Contradicting opinions, however, were published with respect to maximum burial depths and thicknesses of now-eroded sedimentary rocks. Füchtbauer and Müller (1970) argued that the thermo-metamorphic alteration of Carboniferous sandstones in the area of

Y. Senglaub · R. Littke (✉)
Institute of Geology and Geochemistry of Petroleum and Coal, RWTH Aachen University, Lochnerstr. 4-20, 52056 Aachen, Germany
E-mail: littke@lek.rwth-aachen.de

M. R. Brix
Institut für Geologie, Mineralogie und Geophysik, Ruhr-Universität Bochum, 44780 Bochum, Germany

Bramsche could reflect a maximum burial depth of 8,000 m. Corresponding to seismic velocity measurements on Carboniferous sedimentary rocks in the vicinity of the Bramsche anomaly, a possible uplift by 6,000 m for the centre of the LSB was assumed by Brink (2002). More recent evaluations in the Ibbenbüren area led to the estimation of 4,500 m subsidence (Thiermann 1980; Drozdzewski 1988), whereas Baldschuhn and Kockel (1999) concluded an uplift of 8,000 m according to thickness extrapolations for this area. Based on reconstructions of missing layer thicknesses, Nodop (1971) in contrast proposed a maximum burial depth of the LSB of only up to 3,500 m followed by inversion exhumation.

Detailed numerical modelling studies using data from several wells were published for areas east and west of the Bramsche Massif. For an area situated between the Bramsche Massif and The Netherlands (Figs. 1, 2), Leischner et al. (1993) suggested enhanced heat flows during maximum burial, but the absolute values were still very similar to those observed at present (about 80 mW/m^2) at the southern margin of the LSB. The study was based on fluid inclusion studies, fission track data, maturity-vs-depth profiles, and numerical modelling. Using a similar approach, Petmecky et al. (1999) falsified the theory of an igneous intrusion in the area of Uchte, east of the Bramsche Massif (Fig. 2). Instead, he postulated that deep burial during Early Cretaceous times followed by Late Cretaceous/Tertiary uplift was responsible for high maturation. A possible mechanistic explanation for this evolution would be the development of a half-graben followed by inversion (McClay 1995).

This study has the overall objective to reconstruct the thermal and burial history of the southern part of the LSB by testing different scenarios of basin subsidence and uplift including emplacement of igneous intrusions. Data from six wells and two pseudo-wells were used to establish numerical 1D models which were calibrated by vitrinite reflectance data. The major focus is on the period of deepest burial when maximum temperatures prevailed and on the following uplift period, that is, on the Cretaceous. The study is part of the scientific priority programme 'Dynamics of Sedimentary Systems under varying stress regimes: the Central European Basin System' of the DFG.

Geological background

The LSB is situated at the southern margin of the Central European Basin System and flanks to the north the London–Brabant, Rhenish, and Bohemian Massifs. The LSB represents an E–W-striking, highly differentiated Meso–Cenozoic basin (Betz et al. 1987; Baldschuhn et al. 1991; Kockel et al. 1994) and was initiated by rifting and/or thermal subsidence of the lithosphere

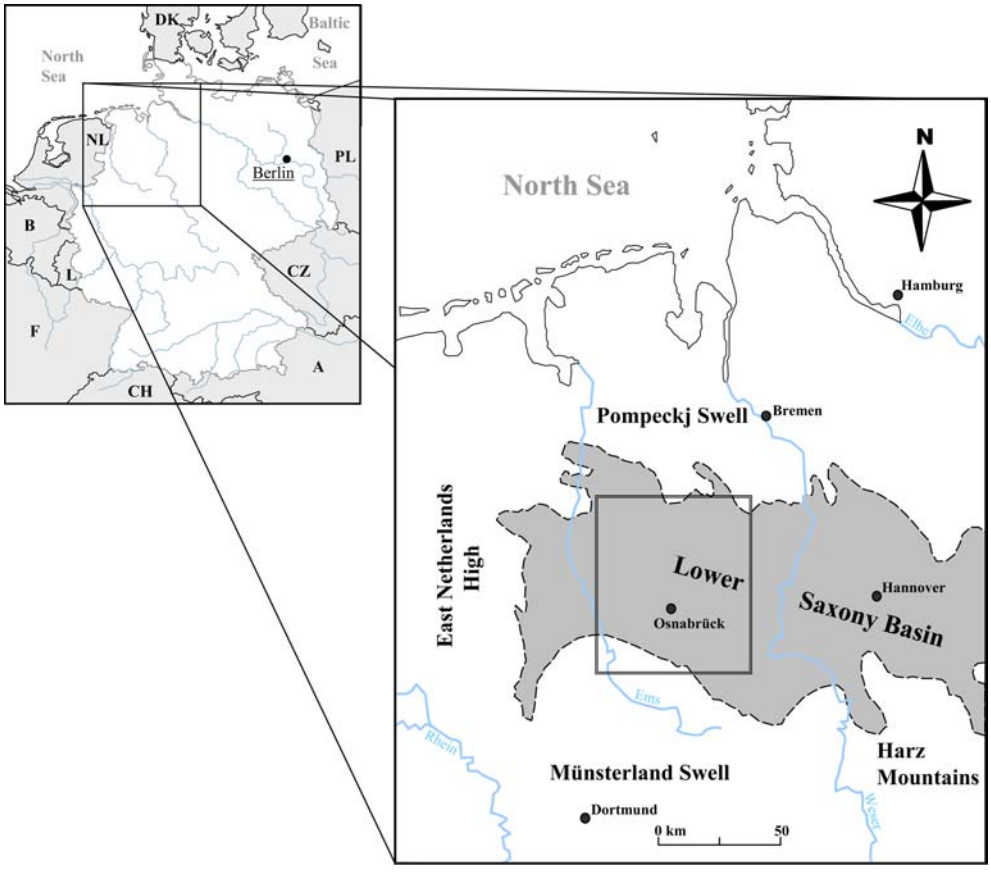

Fig. 1 Location of the study area in western Europe

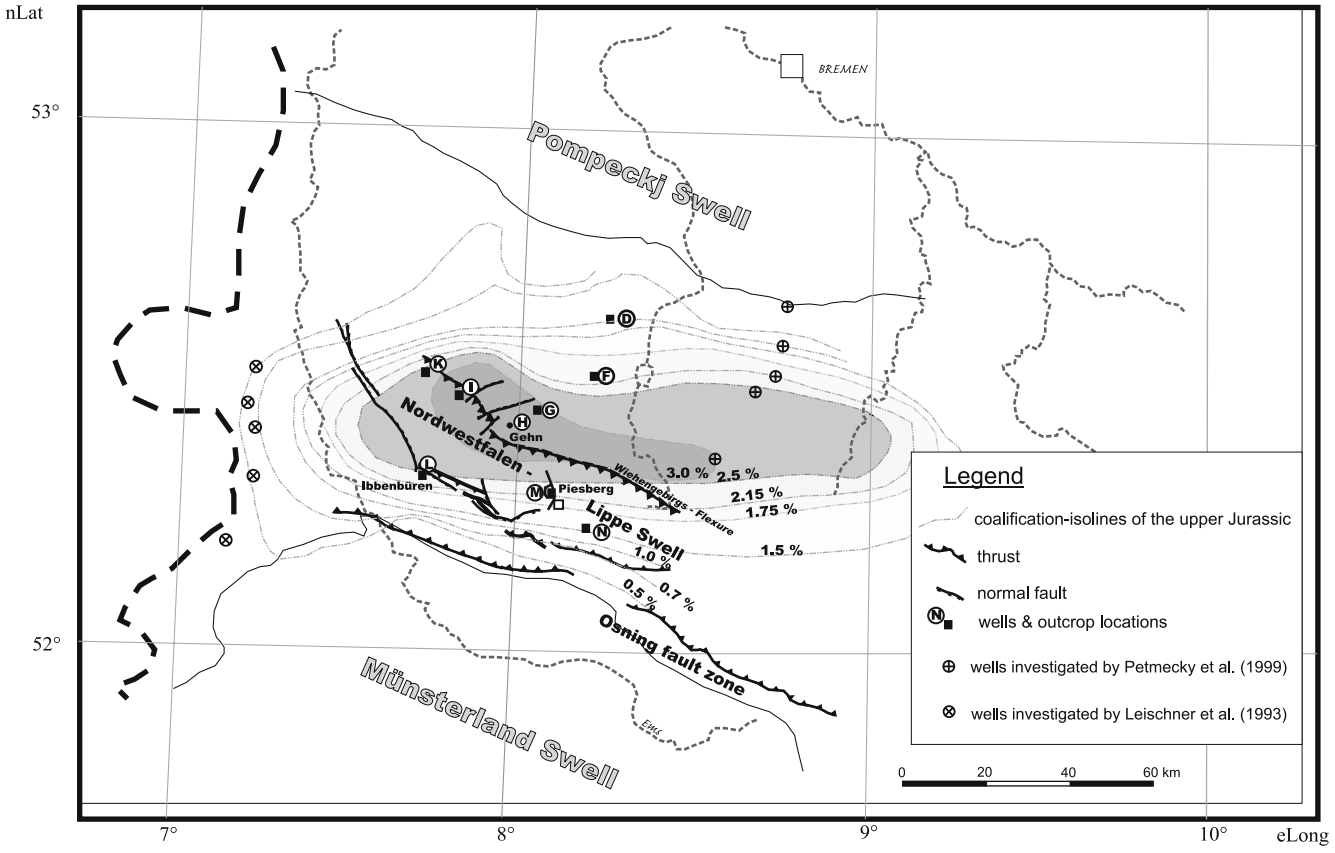

Fig. 2 Coalification map of the Late Jurassic based on Bartenstein et al. (1971)

during the Permian. The rifting centre was situated north of the LSB (Plein 1978; Ziegler 1982; Bachmann and Grosse 1989; Neunzert et al. 1996; van Wees et al. 2000). Economically important is the basement consisting of marine Devonian and Lower Carboniferous and coal-bearing Upper Carboniferous rocks which act as important source rocks for natural gas (Littke et al. 1995). Based on rift and wrench tectonics in the Late Jurassic, the LSB began to subside rapidly, bordered in the south by the Rhenish Massif, in the west by the Central Netherlands High, in the north by the Pompeckj Swell, and in the east by the N–S-trending Gifhorn Trough (Fig. 1; Kockel et al. 1994). During Coniacian and Santonian times, the LSB was inverted and existing normal faults became reactivated and transformed into steep thrusts and reverse faults (Baldschuhn and Kockel 1999). A general overview on the stratigraphy is given in Fig. 3.

During the Late Carboniferous, the study area was situated in a foredeep of the rising Variscan mountain belt being formed towards the south. A thick coal-bearing sedimentary sequence was deposited and partly eroded during the Variscan (Hercynian) orogeny, that is, during the latest Carboniferous and/or earliest Permian (Süss 1996). The Upper Carboniferous deposits correspond to a deltaic system and are characterized by fluvial and marine sedimentary rocks (mainly silt- and sandstones) with intercalations of coal. Geologically, the folded Upper Carboniferous rocks are regarded as the basement of the Central European Basin System including the LSB, but they are not the economic basement since they provide major gas source rocks and even reservoir rocks to the petroleum system. Rotliegend deposits marking the opening of the Central European Basin System are rare in the LSB and restricted to its northern part; they exist in great thickness and with abundant volcanoclastic material in the area of the Pompeckj Swell further north (Fig. 1).

In the LSB, the transgression of the hypersaline Zechstein Sea led to the deposition of the basal sediments covering the slightly folded Upper Carboniferous units. The related sedimentary rocks mainly consist of salt, anhydrite, dolomite, and limestone with decreasing thickness towards the south. During Triassic times, the LSB received thick post-rift sediments with clastic material predominating during the Lower and Upper Triassic (Bunter and Keuper) and carbonates representing the Mid Triassic (Muschelkalk). The thickness of Triassic deposits was governed by the existence of several NNE-striking depressions and swells. In the study area, the thickness of Bunter clastics increases from SE (Hunte Swell, Trusheim 1961) to NW (Emsland area). Minor uplift events followed by terrestrial and fluvial intercalations affected deposition during Keuper time.

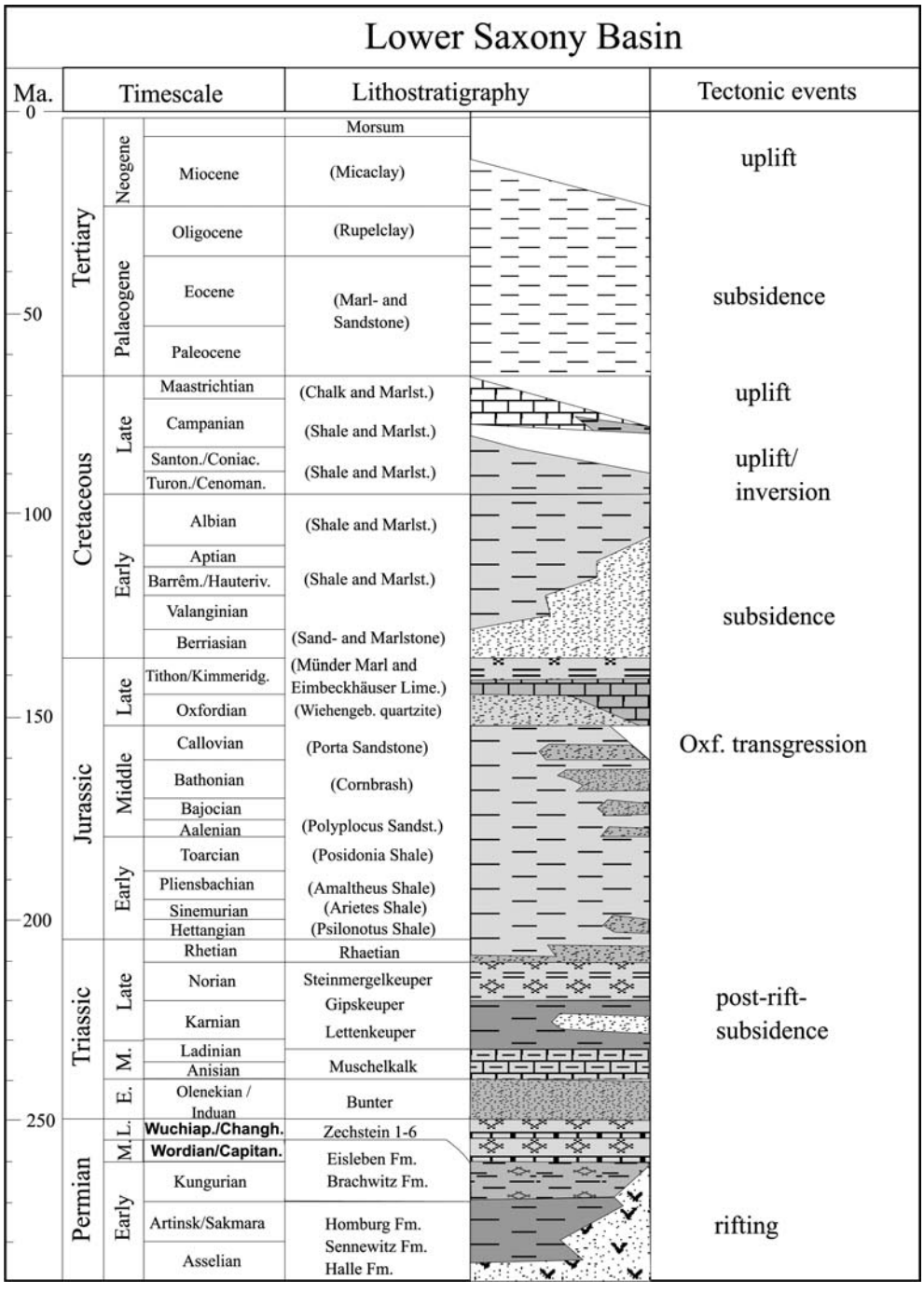

Fig. 3 Generalized stratigraphy of the LSB from Permian until recent times based on the German Stratigraphic Commission (2002)

During the Jurassic, the depositional environment shifted to shallow marine. This evolution led to the deposition of a sedimentary succession consisting of shales, marls, carbonates, and sands, the latter being more abundant in the Upper Jurassic (Gramann et al. 1997). Regression of the sea during latest Jurassic and earliest Cretaceous times led to terrestrial intercalations ('Wiehengebirgsquarzit', Wealden facies). Based on strong vertical and horizontal movements along the southern fault-bounded border of the LSB, thick shallow marine to terrestrial sequences developed in the Tithonian ('Münder Marl' and 'Serpulit') as well as in the lowermost Cretaceous ('Wealden'; Skupin 2003).

Up to the Barrêmian and earliest Aptian, dark-coloured clastic sediments with commonly high concentrations of organic matter were deposited. A change of the depositional environment towards more 'open-marine' conditions and warmer (Tethyan) water occurred during the early Aptian. Later, light-coloured marls predominated the sedimentary sequence (Mutterlose 1992; Jendrzejewski 1995).

Due to inversion tectonics in the Coniacian/Santonian, the LSB developed to the Lower Saxony Tectogene. During this inversion, the basin fill was uplifted and overthrusted on the Münsterland Swell to the south as well as on the Pompeckj Swell to the north (Drozdzewski 2003). Due to subsequent erosion, the sedimentary record of the Upper Cretaceous was almost lost. Sedimentation resumed again in the Paleocene–Oligocene. From the Miocene onwards, minor erosion took place in the LSB.

Samples and methods

Samples

Organic matter-rich sedimentary rocks from different stratigraphic units were sampled for petrological investigations to obtain information on the regional maturity pattern. With respect to cores and cuttings from boreholes, an attempt was made to sample as many stratigraphic intervals as possible. This goal could not always be achieved, since for some wells sample material was not continuously available over the entire depth range. Collected samples consist mainly of coals and organic matter bearing dark shales. About 30 samples yielded valid new vitrinite reflectance data (Table 1).

Vitrinite reflectance

Reflectance of coal macerals has long been used to evaluate coal rank (Taylor et al. 1998). Vitrinite is the maceral most often used for this purpose because its optical properties alter more uniformly during rank advance than do those of other maceral groups. Moreover, vitrinite reflectance has been the major calibration parameter for modelling the thermal history of sedimentary rocks (Radke et al. 1997) since the results of Lopatin were published (Lopatin 1971; Waples 1980).

Vitrinite reflectance measurements were performed at randomly oriented vitrinite grains using a Zeiss universal microspectrometer and followed established procedures as described in Taylor et al. (1998) with two isotropic glass standards of 0.89 and 1.70% reflectance. Random vitrinite reflectance values measured on dispersed organic material often differ from those measured on coals and show more scatter (Scheidt and Littke 1989). Causes for these deviations include measurements of allochthonous vitrinites of higher maturity, measurements on inertinite or solid bitumen which are difficult to distinguish from vitrinite at high coalification levels, and artefacts due to small particle size, and a lower quality of the polished surface. The standard deviation of vitrinite reflectance values should be less than 0.1–0.2% for mean reflectance values below 2.0% and increase with maturity; however, measurements on dispersed organic material can show standard deviations exceeding these values. Standard deviations obtained in the framework of this study are summarized in Table 1.

The complete vitrinite reflectance data set consists of outcrop and core samples and is a compilation of

Table 1 Results of vitrinite reflectance measurements. Northing and Easting refer to Gauss-Küger coordinates

Location	Depth (m)	Northing	Easting	Lithology	Stratigraphy	VRr (%)	SD (%)	Meas. points
E-Gehn	Surface	58 12 975	34 25 750	Coal	Oxfordian	3.56	0.256	60
E-Gehn	Surface	58 12 975	34 25 750	Coal	Oxfordian	3.76	0.235	59
W-Gehn	Surface	58 11 075	34 23 700	Coal	Oxfordian	4.09	0.147	50
Ibbenbüren	Surface	57 97 917	34 10 482	Coal	Westphalian C	1.50	0.075	60
Piesberg	Surface	57 98 775	34 32 675	Coal	Westphalian C	4.69	0.16	50
Piesberg	Surface	57 98 800	34 33 075	Coal	Westphalian C	4.73	0.163	51
Piesberg	Surface	57 98 725	34 33 775	Coal	Westphalian C	4.31	0.151	51
Piesberg	Surface	57 98 725	34 33 775	Coal	Westphalian C	4.55	0.252	60
Piesberg	Surface	57 98 725	34 33 775	Coal	Westphalian C	4.74	0.144	80
Vehrte	Surface	58 02 075	34 42 975	Shale	Toarcian	1.94	0.28	50
Well G	80	–	–	Shale	up. Malm	2.65	0.318	48
Well G	205	–	–	Shale	up. Malm	3.03	0.313	14
Well G	295	–	–	Shale	Kimmeridgian	3.07	0.298	22
Well G	490	–	–	Shale	Kimmeridgian	3.13	0.209	10
Well G	620	–	–	Shale	Oxfordian	3.06	0.262	13
Well G	770	–	–	Shale	Dogger	3.39	0.204	12
Well G	930	–	–	Shale	Dogger	3.27	0.298	25
Well G	1,755	–	–	Shale	Hettangian	3.99	0.36	35
Well G	1,872	–	–	Shale	up. Keuper	4.26	0.297	50
Well G	1,930	–	–	Marlstone	mid. Keuper	4.47	0.272	35
Well G	2,222	–	–	Marlstone	up. Muschelk.	4.51	0.21	50
Well G	2,587	–	–	Siltstone	mid. Bunter	4.65	0.171	41
Well G	3,467	–	–	Shale	Westphalian D	4.50	0.242	30
Well G	3,486	–	–	Sandstone	Westphalian D	4.64	0.142	50
north of Well E	1,807	–	–	Shale	Bajocian	0.79	0.128	63
Well E	1,976	–	–	Shale	Toarcian	0.93	0.152	67
Well E	2,318	–	–	Shale	mid. Bunter	1.37	0.374	29
Well E	3,538	–	–	Shale/siltstone	Carbonif.	1.99	0.199	16

own measurements (Table 1), industrial data, data from the VIDABA (vitrinite data base of BGR, Hannover), and numerous published data (Bartenstein et al. 1971; Teichmüller et al. 1979; Teichmüller and Teichmüller 1985; Lommerzheim 1988; Günther et al. 1998). Stratigraphically, the data set covers Westphalian B to Tertiary sedimentary rocks.

Thermal modelling

Since the early publications of Lopatin (1971), Waples (1980), and Welte and Yükler (1981), the numerical simulation of burial, erosion, and thermal histories of sedimentary basins became a widely used method in geology, particularly in petroleum exploration. Here, 1D thermal modelling was applied using PetroMod software of IES, Jülich, Germany. Thermal and burial histories were calibrated by comparing measured and calculated vitrinite reflectance data (Fig. 4). For the calculation of vitrinite reflectance, the kinetic EASY%Ro algorithm (Sweeney and Burnham 1990) was used. For a detailed discussion of the basin modelling concept and limitations see Poelchau et al. (1997) and Yalcin et al. (1997).

Discretization of geologic history, heat flow, and erosion

Each numerical simulation has to be based on a conceptual model, which describes basic geologic processes, that is, deposition, non-deposition, and erosion during the geologic evolution of the study area, resulting in a basic set of input data for the simulation (Welte and Yalcin 1988). One major problem of the conceptual model is the reconstruction of time spans which are not represented by a physical record of sedimentary rocks, either due to sedimentation followed by erosion or due to periods of non-deposition.

The following description of the geologic history of the LSB is mainly based on the work of Thiermann (1970), Klassen (1984), Baldschuhn et al. (1999, 2001), Mutterlose and Bornemann (2000), and the Geologischer Dienst NRW (2003) and serves as base for the conceptual model (see Table 2).

As basement of the sedimentary sequence, the Westphalian B was selected which had been cored in the Ibbenbüren area. About 1,500 m coal-bearing siliciclastic sedimentary rocks (Westphalian C and D) cover the basement, also documented in the Ibbenbüren area wells. Between the latest Carboniferous and the earliest

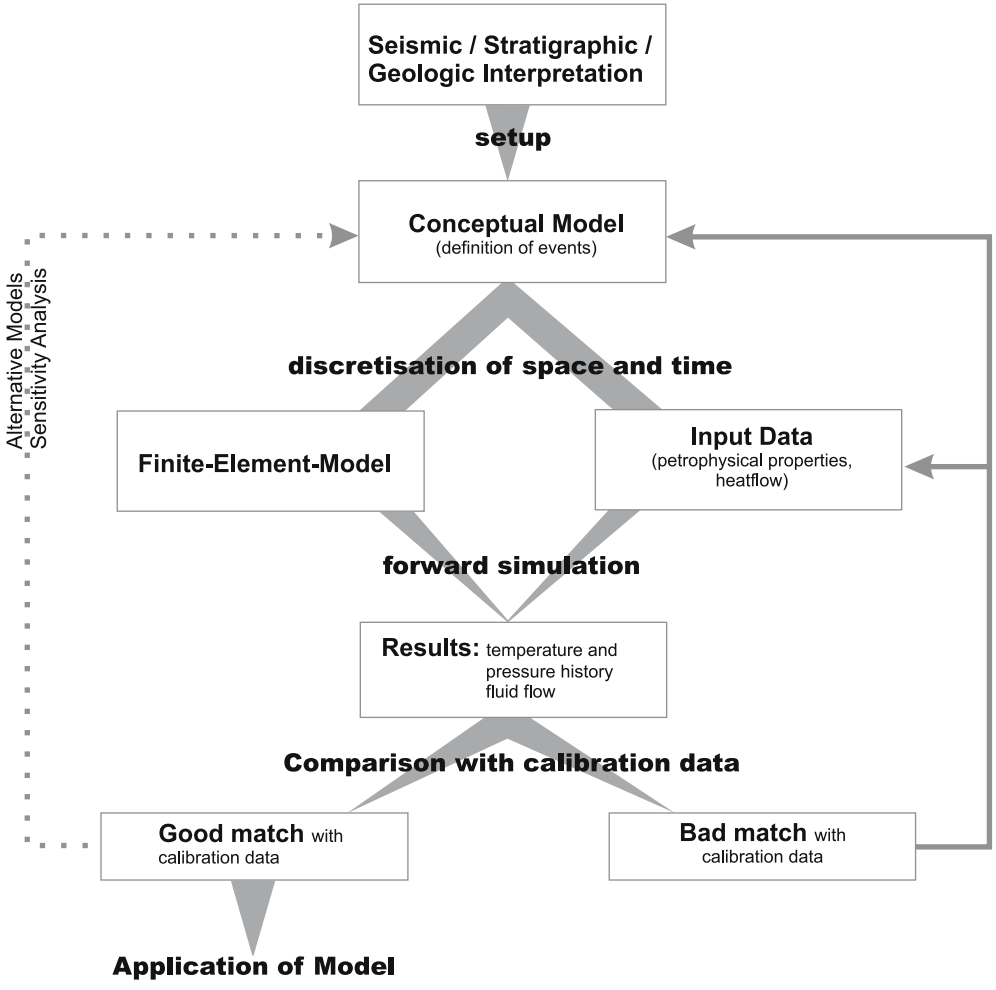

Fig. 4 Scheme of the numerical modelling procedure (see text for further explanation)

Table 2 Input data for modelling of burial, erosion, and temperature of Well G (Fig. 2)

Event	Name	Thickness [m]	Erosion [m]	Deposition Age		Erosion Age		Lithology	Water depth [m]	SWI [°C]	Heatflow [mW/m^2]
				From [ma]	To [ma]	From [ma]	To [ma]				
46	Quaternary	55		1.8	0.00			Sandstone	0	5	60
45	*Oligocene*		*−70*			*3.00*	*1.8*		0	16	60
44	*Miocene*		*−84*			*5.3*	*3.00*		*0*	16	60
43	Miocene	84		23.80	5.3			mixing	30	16	60
42	Oligocene	70		33.70	23.80			mixing	30	17	60
41	*Campanian*		*−230*			*71.30*	*33.70*		*0*	17	60
40	Campanian	230		73.00	71.30			SHALEcarb	30	18	60
39	*Malm*		*−160*			*74.40*	*73.00*		*0*	18	63
38	*Münder Mergel*		*−900*			*75.80*	*74.40*		*0*	18	63
37	*Serpulit Fm.*		*−50*			*77.20*	*75.80*		*0*	18	63
36	*Wealden*		*−700*			*78.60*	*77.20*		*0*	19	63
35	*Valanginian*		*−300*			*80.00*	*78.60*		*0*	19	63
34	*Hauterivian*		*−400*			*81.40*	*80.00*		*0*	19	63
33	*Barremian*		*−300*			*82.80*	*81.40*		*0*	19	63
32	*Aptian*		*−275*			*84.20*	*82.80*		*0*	19	63
31	*Albian*		*−375*			*85.60*	*84.20*		*0*	19	63
30	*upper Cretaceous*		*−525*			*87.00*	*85.60*		*0*	19	63
29	upper Cretaceous	525		98.50	87.00			SHALEcalc	80	20	60
28	Albian	375		112.20	98.50			SHALEcalc	100	19	60
27	Aptian	275		120.00	112.20			SHALEcalc	100	18	60
26	Barremian	300		127.00	120.00			SHALEcalc	100	18	60
25	Hauterivian	400		132.00	127.00			SHALEcalc	75	18	60
24	Valanginian	300		137.00	132.00			SHALEcalc	50	18	60
23	Wealden	700		140.00	137.00			mixing	5	19	60
22	Serpulit Fm.	50		141.00	140.00			mixing	10	19	60
21	Münder Marl	900		144.00	141.00			mixing	10	19	60
20	Malm	341		146.00	144.00			mixing	20	19	60
19	Kimmeridgian	314		152.50	146.00			mixing	10	18	60
18	Oxfordian	95		156.50	152.50			mixing	10	17	60
17	*Dogger*		*−50*			*161.50*	*156.50*		*0*	17	60
16	Dogger	525		178.00	161.50			mixing	75	14	60
15	Liassic	725		200.00	178.00			mixing	100	13	60
14	Rhät	84		209.00	200.00			mixing	5	15	60
13	mid Keuper	243		232.50	209.00			mixing	5	15	60
12	lower Keuper	36		235.00	232.50			mixing	5	15	60
11	upper Muschelkalk	36		238.50	235.00			mixing	30	9	60
10	mid. Muschelkalk	101		240.00	238.50			mixing	15	9	60
9	lower Muschelkalk	102		243.00	240.00			Marl	30	9	60
8	upper Bunter	133		244.50	243.00			mixing	20	6	60
7	mid. Bunter	79		246.00	244.50			Shale	15	6	60
6	lower Bunter	234		251.00	246.00			mixing	15	4	60
5	Zechstein	573		258.00	251.00			mixing	15	4	60
4	*Westphalian D*		*−490*			*305.00*	*258.00*		*0*	1	75
3	Westphalian D	650		308.00	305.00			mixing	5	3	75
2	Westphalian C	850		311.00	308.00			mixing	5	3	60
1	Westphalian B	850		313.50	311.00			mixing	5	4	60

Permian, a period of non-deposition was assumed for a large part of the basin. Probably, sedimentation followed by erosion is a more likely scenario for this time span as is well recorded for the Münsterland Swell further south (Littke et al. 2000). However, the thermal effect of this possible depositional period was clearly overwhelmed by Mesozoic events, especially of Cretaceous time. Furthermore, the effect of this Late Carboniferous depositional event on gas generation from the coal-bearing Westphalian is beyond the scope of this study. Therefore, to keep the conceptual model as simple as possible, non-deposition was used as input data for this period.

Eruptive rocks were documented in the lithologic log of Well D and Well A5 (Petmecky et al. 1999) and point to a volcanic event during Rotliegend times in the northern part of the study area, coinciding with the syn-rift stage of the Central European Basin System and certainly affecting the then deposited sequence through elevated heat flow. Zechstein thickness increases from 200 m in the southern part up to 930 m in the northern part of the basin. The Triassic is characterized by short tectonic events reflected by discontinuities (e.g. Hardegsen- and Solling-Diskordanz; Steinmergelkeuper-Diskordanz). These events were short and insignificant with respect to burial and thermal history and, therefore,

Table 3 Lithological composition and physical rock properties assigned to layers used in simulations

	Sand./ S.congl. [%]	Silt./sandy [%]	Shale [%]	Marlstone [%]	Limestone [%]	Dolomite [%]	Anhyd./ Gyps. [%]	Salt [%]	Coal [%]	Matrix Density [kg/m^3]	Compressibility [1/10 GPa]		Matrix Thermal Conductivity [W/mK]		Matrix Heat Capacity [cal/gK]	
											Min	Max	20°C	100°C	20°C	100°C
Well D																
Quaternary	100	–	–	–	–	–	–	–	–	2660.0	10.0	500.0	3.12	2.64	0.178	0.209
Eocene	8	7*	52	33	–	–	–	–	–	2669.6	10.0	36249.0	1.86	1.78	0.210	0.255
Hauterivian	–	–	50	50	–	–	–	–	–	2667.5	10.0	51961.5	1.72	1.65	0.213	0.258
Valanginian	–	–	50	50	–	–	–	–	–	2667.5	10.0	51961.5	1.72	1.65	0.213	0.258
Wealden	–	–	50	43	6	–	–	–	–	2661.1	10.0	37296.0	1.77	1.69	0.211	0.256
Upper Malm	–	–	45	44	–	6	5/	–	–	2686.9	8.9	23526.7	1.91	1.80	0.210	0.253
Kimmeridgian	–	–	–	–	60	40	–	–	–	2760.4	10.0	184.0	3.19	2.80	0.198	0.225
Dogger	6	–	50	39	5	–	–	–	–	2670.9	10.0	32311.6	1.84	1.75	0.210	0.255
Lias	5	–	57	33	5	–	–	–	–	2673.3	10.0	34323.9	1.88	1.79	0.211	0.255
Upper-mid Keuper	50	–	25	25	–	–	–	–	–	2666.3	10.0	9936.1	2.11	1.95	0.202	0.243
Lower Keuper	8	–	58	34	–	–	–	–	–	2670.3	10.0	41278.2	1.84	1.76	0.211	0.256
Upper Muschelk.	–	–	–	46	54	–	–	–	–	2699.4	10.0	348.9	2.54	2.34	0.201	0.235
Mid Muschelk.	–	–	–	15	13	2	2/	68	–	2337.9	2.0	15.8	4.46	3.84	0.204	0.219
Lower Muschelk.	–	–	–	47	43	–	–	–	–	2701.1	10.0	335.9	2.56	2.36	0.201	0.235
Upper Bunter	–	–	–	–	–	–	2/	98	–	2168.5	1.0	4.3	5.65	4.73	0.206	0.212
Mid Bunter	27	26	24	23	–	–	–	–	–	2666.3	10.0	9010.2	2.14	1.98	0.202	0.243
Lower Bunter	–	22	36	33	9	–	–	–	–	2671.1	10.0	14889.1	1.98	1.86	0.206	0.248
Zechstein	–	–	8	–	2	–	44/	46	–	2516.2	1.3	9.3	4.79	4.03	0.192	0.206
New Red	–	50*	50*	–	–	–	–	–	–	2670.5	10.0	11619.0	2.24	2.11	0.203	0.245
Westphalian D/C	/11	52	37	–	–	–	–	–	–	2668.1	10.0	3192.6	2.43	2.21	0.197	0.236
Well E																
Tertiary	–	14 *	86	–	–	–	–	–	–	2678.0	10.0	46004.9	2.02	1.94	0.211	0.256
Aptian	–	–	54	46	–	–	–	–	–	2667.5	10.0	51961.5	1.72	1.65	0.213	0.258
Barrêmian	–	–	39	61	–	–	–	–	–	2674.2	10.0	4417.3	1.90	1.81	0.210	0.252
Hauteriv./Valan.	–	–	23	77	–	–	–	–	–	2660.0	10.0	47665.1	1.59	1.52	0.212	0.258
Wealden	–	–	92	–	–	–	–	–	8 (sh.)	2663.5	10.0	54112.5	1.96	1.88	0.212	0.257
Upper Malm	–	–	86	–	–	5	9/	–	–	2704.8	7.9	17439.4	2.24	2.11	0.209	0.250
Upper Kimmeridgian	–	–	93	–	1	–	6	–	–	2690.5	8.7	31736.9	2.10	2.00	0.210	0.254
Mid-lower Kimmdg.	1	–	94	–	5	–	–	–	–	2681.3	10.0	42389.3	2.02	1.94	0.212	0.256
Bathonian	3	–	–	97	–	–	–	–	–	2655.1	10.0	39317.4	1.53	1.46	0.211	0.257
Bajocian	–	3	97	–	–	–	–	–	–	2679.6	10.0	54096.5	2.00	1.92	0.212	0.257
Upper Bunter	–	–	48	–	–	–	10	42	–	2478.6	3.0	404.2	3.37	3.02	0.206	0.232
Mid – lower Bunter	–	39	61	–	–	–	–	–	–	2673.8	10.0	13048.3	2.32	2.17	0.203	0.244
Zechstein 4-2	–	–	5	–	–	–	/22	73	–	2216.8	1.1	5.6	4.03	3.48	0.237	0.247
Zechstein 1	–	–	–	–	–	13	87/	–	–	2847.9	1.4	7.4	4.64	3.85	0.178	0.195
New Red-Carbonif.	93	7	–	–	–	–	–	–	–	2660.0	10.0	500.0	3.12	2.64	0.178	0.209
Well F																
Quaternary	68	–	29	3	–	–	–	–	–	2666.0	10.0	2102.4	2.72	2.40	0.189	0.224
Tertiary	91	–	–	9	–	–	–	–	–	2662.5	10.0	615.1	3.03	2.59	0.181	0.213
Münder Marl	–	–	17	–	–	–	10/13	60	–	2331.4	1.5	17.8	3.75	3.25	0.222	0.237
Eimb. Limest.	–	–	–	38	–	–	4/58	–	–	2442.0	2.5	110.1	1.51	1.42	0.293	0.320
Gigas-Fm.	–	–	28	72	–	–	–	–	–	2662.5	10.0	49056.2	1.63	1.56	0.212	0.258

Table 3 (Contd.)

Upper Kimmeridgian	–	2	6	92	–	–	–	–	–	2656.8	10.0	44228.9	1.54	1.47	0.212	0.258
Mid Kimmeridgian	16	–	–	84	–	–	–	–	–	2655.8	10.0	21904.5	1.69	1.58	0.207	0.250
Bathonian	12	–	–	88	–	–	–	–	–	2655.6	10.0	26224.3	1.64	1.54	0.208	0.252
Well G																
Upper Malm	–	–	23	61	–	–	16	–	–	2690.5	7.1	11933.7	1.91	1.79	0.207	0.248
Kimmeridgian	7	2	43	48	–	–	–	–	–	2665.5	10.0	32193.2	1.80	1.71	0.209	0.253
Oxfordian	68	3	–	29	–	–	–	–	–	2658.5	10.0	1928.6	2.50	2.20	0.188	0.224
Dogger	–	–	49	51	–	–	–	–	–	2667.5	10.0	51961.5	1.72	1.65	0.213	0.258
Lias	–	–	93	7	–	–	–	–	–	2678.8	10.0	59143.1	1.95	1.88	0.213	0.258
Upper Keuper	38	4	58	–	–	–	–	–	–	2672.0	10.0	8840.5	2.37	2.17	0.199	0.238
Mid Keuper	–	–	77	17	–	–	6	–	–	2684.8	8.9	35530.9	1.99	1.90	0.211	0.255
Lower Keuper	–	16	84	–	–	–	–	–	–	2677.8	10.0	35747.2	2.06	1.97	0.210	0.254
Upper Muschelk.	–	–	–	63	34	3	–	–	–	2702.5	10.0	462.8	2.49	2.31	0.203	0.238
Mid Muschelk.	–	–	–	–	–	–	76	24	–	2684.4	1.0	4.0	5.01	4.15	0.182	0.195
Upper Bunter	–	–	–	78	–	–	–	22	–	2556.0	6.3	6966.0	1.96	1.82	0.211	0.249
Mid Bunter	–	–	100	–	–	–	–	–	–	2680.0	10.0	60000.0	1.98	1.91	0.213	0.258
Lower Bunter	39	61	–	–	–	–	–	–	–	2667.3	10.0	2713.2	2.48	2.25	0.192	0.229
Zechstein	–	–	–	–	–	4	36	60	–	2435.4	1.1	4.7	5.27	4.39	0.194	0.204
Westphalian D	68/1	17	13	–	–	–	–	–	1	2654.6	10.0	1486.7	2.73	2.39	0.186	0.221
Well I																
Mid Muschelk.	–	12	10	–	24	–	54/	–	–	2788.4	2.9	65.9	3.65	3.15	0.187	0.212
Lower Muschelk.	–	–	–	5	95	–	–	–	–	2708.9	10.0	164.4	2.80	2.54	0.196	0.224
Upper Bunter	–	–	54	–	–	–	46/	–	–	2758.2	3.5	719.7	2.98	2.67	0.195	0.226
Mid Bunter	9	47	44	–	–	–	–	–	–	2675.8	10.0	21430.3	2.08	1.97	0.208	0.252
Lower Bunter	–	13	87	–	–	–	–	–	–	2678.1	10.0	38302.7	2.05	1.96	0.210	0.254
Zechstein	–	–	5	–	–	17	45/	33	–	2611.4	1.7	13.1	4.67	3.92	0.191	0.207
Westphalian D	/1	75	24	–	–	–	–	–	–	2668.6	10.0	4275.7	2.43	2.21	0.197	0.236
Well K																
Quaternary	/71	–	–	29	–	–	–	–	–	2660.7	10.0	1372.7	2.41	2.20	0.192	0.229
Miocene	–	20	–	80	–	–	–	–	–	2657.0	10.0	23895.8	1.67	1.57	0.208	0.252
Oligocene	–	20	–	80	–	–	–	–	–	2657.0	10.0	23895.8	1.67	1.57	0.208	0.252
Upper Eocene	/1	7	–	92	–	–	–	–	–	2655.8	10.0	34328.4	1.57	1.49	0.210	0.256
Lower Eocene	–	–	–	100	–	–	–	–	–	2655.0	10.0	45000.0	1.50	1.43	0.212	0.258
Hettg./Sinem.	–	–	99	1	–	–	–	–	–	2679.8	10.0	59827.6	1.97	1.90	0.213	0.258
Upper Keuper	–	77	23	–	–	–	–	–	–	2668.4	10.0	4203.5	2.43	2.21	0.197	0.236
Mid Keuper	–	2	–	83	12	–	3/	–	–	2687.9	9.3	1409.3	2.18	2.05	0.207	0.246
Lower Keuper	–	–	71	–	29	–	–	–	–	2685.8	10.0	15388.4	2.12	2.02	0.210	0.252
Upper Muschelk.	–	–	–	34	66	–	–	–	–	2702.2	10.0	280.0	2.61	2.40	0.199	0.231
Mid Muschelk.	–	–	–	18	5	45	32/	–	–	2801.6	4.8	165.2	3.42	2.94	0.194	0.221
Lower Muschelk.	–	–	–	10	76	14	–	–	–	2722.1	10.0	285.0	2.77	2.49	0.198	0.227
Upper Bunter	–	–	84	13	3	–	–	–	–	2677.4	10.0	50208.3	1.92	1.85	0.213	0.257
Mid Bunter	–	34	63	–	2	–	1/	–	–	2677.4	9.8	15533.1	2.19	2.06	0.205	0.247
Lower Bunter	–	18	82	–	–	–	–	–	–	2674.9	10.0	17481.4	2.12	2.00	0.207	0.250
Zechstein	–	–	11	–	2	1	58/	28	–	2635.2	1.4	12.9	4.51	3.81	0.188	0.204
Westphalian D	40/1	15	44	–	–	–	–	–	–	2672.9	10.0	11380.6	2.23	2.08	0.203	0.245

Table 3 (Contd.)

	Sand./ S.congl. [%]	Silt./sandy [%]	Shale [%]	Marlstone [%]	Limestone [%]	Dolomite [%]	Anhyd./ Gyps. [%]	Salt [%]	Coal [%]	Matrix Density [kg/m^3]	Compressibility [1/10 GPa]		Matrix Thermal Conductivity [W/mK]		Matrix Heat Capacity [cal/gK]	
											Min	Max	20°C	100°C	20°C	100°C
Well L																
Westphalian D	49/1	47	3	–	–	–	–	–	–	2668.7	10.0	4069.8	2.35	2.16	0.197	0.236
Westphalian C	59/5	–	34	–	–	–	–	–	2	2650.3	10.0	6126.9	2.30	2.11	0.199	0.239
Westphalian B	43	30	25	–	–	–	–	–	2	2651.1	10.0	7544.1	2.21	2.05	0.200	0.241
Standard lithologies																
Sandstone										2660.0	10.0	500.0	3.12	2.64	0.178	0.209
Siltstone										2672.0	10.0	8000.0	2.14	2.03	0.201	0.242
Shale										2680.0	10.0	60000.0	1.98	1.91	0.213	0.258
Marlstone										2687.0	10.0	940.0	2.23	2.11	0.208	0.248
Limestone										2710.0	10.0	150.0	2.83	2.56	0.195	0.223
Dolomite										2836.0	10.0	250.0	3.81	3.21	0.202	0.229
Anhydrite										2850.0	1.0	4.0	5.69	4.76	0.206	0.212
Gypsum										2300.0	1.0	2.0	1.51	1.41	0.347	0.361
Salt										2160.0	1.0	4.0	5.69	4.76	0.206	0.212
Coal										1680.0	10.0	130000.0	0.50	0.46	0.204	0.248

* mixed with volcanic material

were not included in the conceptual model (Table 2). During Bunter times, the presence of the NNE-striking Hunte Swell resulted in a shift of the depositional centre westwards into the Niederrhein-Ems depression. The cumulative thickness increases from 440 to 891 m in this direction. Overlying Muschelkalk strata are dominated by playa lake sediments with increasing contributions of halite north of the line Veltheim–Lübecke–Hunteburg. Keuper (Upper Triassic) thickness changes from the northern margin (164 m) towards the centre of the basin (363 m), reflecting a different tectonic setting. During the Early Jurassic, a WNW–ESE striking graben evolved. Subsidence was significant in the centre of the basin, where up to 700 m Liassic and 600 m Dogger sediments were accumulated. During the Late Jurassic and earliest Cretaceous, subsidence increased. For example, sedimentary rocks of Berriasian age (upper Münder Marl/Serpulit) are more than 1,000 m thick in the central part of the LSB. Gramann et al. (1997) supposed rift events for the western part of the LSB based on thickness differences of up to 1,000 m in the Münder Marl Formation.

The Berriasian–Barrêmian sequence contains numerous sandstones along the basin margin (Osning sandstone in the south, Bentheim and Gildehaus sandstone in the west). The subsequent early Cretaceous succession is dominated by a clay-rich basin facies indicating high subsidence and high sedimentation rates. A decreasing cumulative thickness of post-Berriasian/Lower Cretaceous deposits from the western part of the LSB (1,950 m) towards the eastern part (1,200 m) is remarkable. In the south, Cretaceous strata are partly or completely eroded. The sequence of Upper Cretaceous sedimentary rocks is incomplete in the LSB with greatest thicknesses of Cenomanian to Santonian sedimentary rocks in the north (up to 525 m). Due to major uplift of the LSB during the Coniacian/Santonian inversion period, erosion of Cretaceous to Carboniferous deposits took place along the Nordwestfalen-Lippe Swell and south of it. With the beginning of the Campanian, tectonic movements almost ceased. Deposits are rare, but recorded for the so-called Dammer Oberkreidemulde (230 m). After a short inversion and erosion phase in Maastrichtian times, sedimentation resumed during the Paleocene–Miocene with approximately 150–200 m sediments. This depositional phase was followed by moderate erosion until recent times.

Conceptual model and input data

Based on the geologic history, about 40 events of deposition, erosion, or non-deposition were defined (Table 2). For each event, absolute ages, thicknesses, lithologies, and related petrophysical properties, sediment–water interface temperatures, and heat flow values were defined. The heat flow history was kept as simple as possible and the heat flow values for the period of maximum temperatures (early Late Cretaceous) were calibrated

using vitrinite reflectance data; they are thus a result of the modelling approach. Surface temperatures were calculated based on the palaeolatitude of central Europe, water depth during deposition, and general climate information (Wygrala 1989). Present-day formation temperatures were used to calibrate the present-day heat flow together with the information on subsurface temperatures (Haenel 1980). Absolute ages were extracted from the geological time scale of the German Stratigraphic Commission (2002). Thicknesses were derived from well data, seismic profiles, and geological maps. Average thermal conductivities were calculated using lithological information and default thermal conductivities for major lithologies taking into account the interlayering of coals, shales, siltstones, sandstones, and conglomerates. Table 3 summarizes lithologic composition and important physical properties of the formations as defined for this study. The temperatures at the sediment–water interface were estimated using information on the palaeolatitude, on the palaeoclimate, and on palaeo water depths of the study area during basin evolution (see Wygrala 1989 for details). These data allow to calculate compaction and temperature field.

Calibration data

For the calibration of the models, vitrinite reflectance data and other maturity parameters, for example, water and volatile matter content of coals (on an ash-free basis) were used. The latter had to be converted into vitrinite reflectance according to Teichmüller et al. (1983). The possible pitfalls of maturity conversions are described in Radke et al. (1997). Vitrinite reflectance data from eight wells are the basis for the calibration of 1D simulations of burial and thermal history.

Results and discussion

Coalification pattern

The coalification pattern in the LSB was already described by Koch and Arnemann (1975) and Teichmüller et al. (1984) who published a coalification map of the Upper Jurassic (Fig. 2). In the framework of the study presented here, additional vitrinite reflectance measurements were performed; results are shown in Table 1. Furthermore, numerical simulation allowed to assess coalification for different stratigraphic levels, for example, for the top of the Carboniferous or the base Cretaceous, even for wells which did not drill these units. The new coalification data basically confirm the previous results, clearly showing an increasing maturity from the margins towards the centre of the LSB. An example is shown in Fig. 5 for the Kimmeridgian surface. This map is a combination of vitrinite reflectance calculated in the course of the numerical modelling and measurements as published by Bartenstein et al. (1971). The map shows a strong maturity increase towards the centre of the basin.

The high maturity of organic matter in the LSB might result from deep burial as suggested by Petmecky et al. (1999) for the area further east. In this case, the coalification isolines of the Upper Jurassic should indicate the palaeo-contours of the LSB at the time of maximum burial before inversion. The different configurations of the coalification isolines at the centre of the basin should suggest fluctuations in thickness of the sequences deposited between the Late Jurassic and Late Cretaceous rather than differences in heat flows during the time of maximum temperatures (see below). For example, strong subsidence and high sedimentation rates have to be assumed for the Wiehengebirgs-flexure zone, which has been interpreted as a swell during Late Jurassic times (Klassen 1991; Baldschuhn et al. 2001).

Thermal modelling: the Ibbenbüren area (southern LSB margin)

A series of simulation runs was carried out for individual wells. Calibration was based on a comparison of measured vitrinite reflectance data and calculated vitrinite reflectance applying the EASY%Ro algorithm (Sweeney and Burnham 1990). This method has been successfully used for calibration purposes and is applicable for maturation values as high as 4.6%VRr. In the study area, some vitrinite reflectance values are, however, higher than 4.6%VRr. These values were integrated into the calculated vitrinite reflectance trend by extrapolating the calculated curve.

In the Ibbenbüren area at the southern border of the LSB, Carboniferous rocks are mined close to the surface, which are in the low volatile bituminous coal/anthracite rank (about 2% vitrinite reflectance VRr). The reasons for this high coalification level have been a matter of debate. Based on numerical basin modelling techniques described above, the contrasting theories about deep burial by 8,000 m of overburden (Baldschuhn and Kockel 1999) and high geothermal gradients corresponding to high heat flows of 155 mW/m^2 (Buntebarth 1985) were tested. First, a best-fit model was developed calibrated by the vitrinite reflectance depth trend which is of high quality for the coal-bearing sequence drilled in Ibbenbüren. The greatest problem for thermal modelling of the Ibbenbüren area is the time gap from the Westphalian until recent times, which is not documented by any sedimentary rocks (Fig. 6a). This time gap permits many different models explaining the high thermal maturity, that is, maximum temperatures could have been reached at any time between the Late Carboniferous and the Late Cretaceous. However, the close proximity to the Bramsche area in the north and the Münsterland Swell in the south suggests that maximum temperatures are either due to Permo Carboniferous events or to Late Cretaceous events (Leischner et al. 1993; Petmecky et al. 1999; Littke et al. 2000).

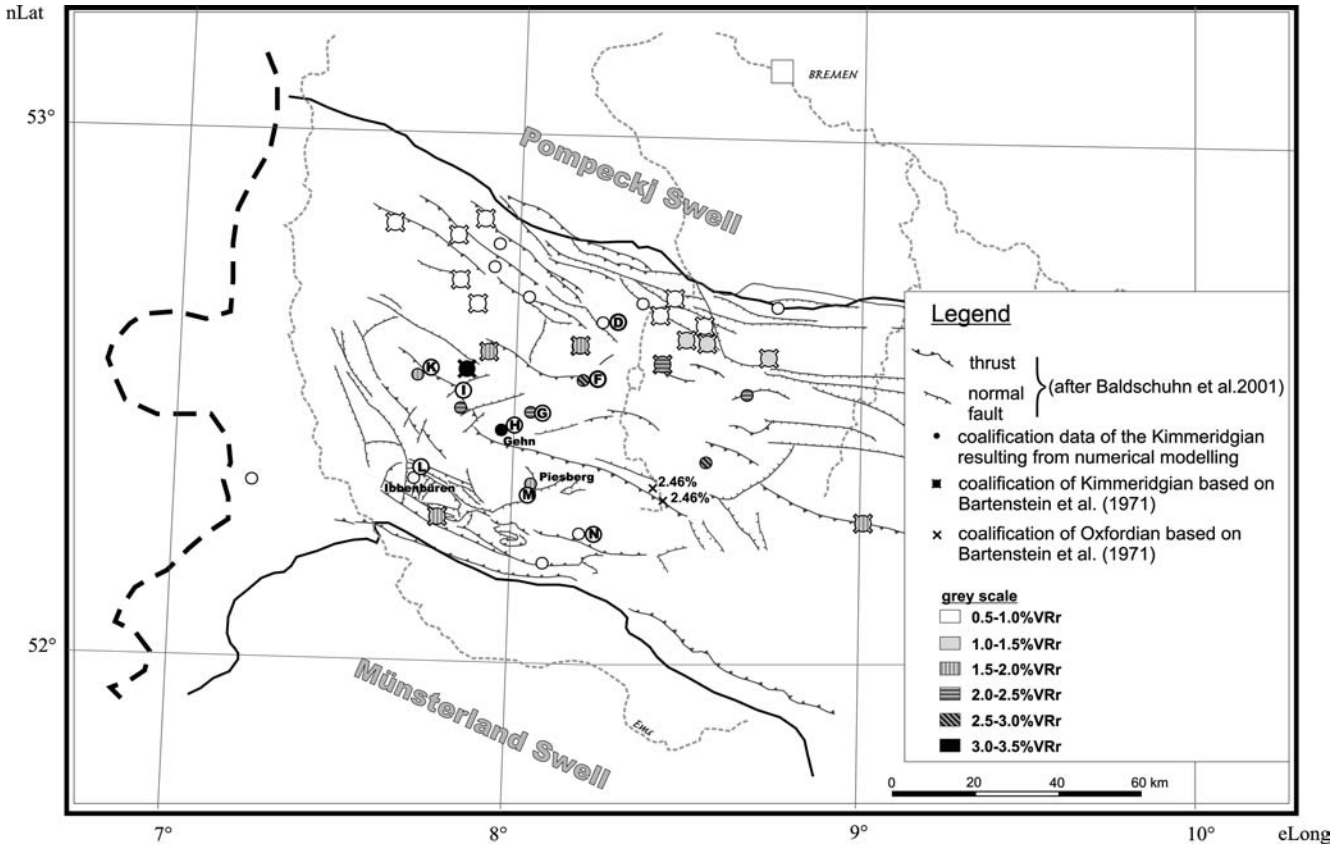

Fig. 5 New coalification map for the Upper Jurassic with major tectonic structures. Maturity information is based on vitrinite reflectance measurements and subsequent calculations using numerical modelling techniques as described in the text

An excellent visual fit between measured and calculated vitrinite reflectance data was achieved by applying a heat flow of 70 mW/m^2 and a thickness of eroded sedimentary rocks of 4,407 m (Fig. 6b). In this model, maximum burial took place during the Late Cretaceous. A maximum burial during Late Carboniferous/Early Permian times would yield a satisfactory fit as well, but would require deposition of more than 4,400 m of additional Stephanian/Upper Permian rocks. This number is far greater than that derived for the adjacent Münsterland Swell (2,800 m, Büker et al. 1995; Littke et al. 2000), where maximum burial occurred during latest Carboniferous/Early Permian. Accordingly, such a scenario of maximum temperatures during the Carboniferous/Permian is not probable for the Ibbenbüren area.

The thickness of the Permian-to-Jurassic sequence was deduced from the thickness in adjacent areas, especially from the Teutoburger Wald area (GK 25 Tecklenburg). In addition, 2,130 m of Cretaceous sedimentary rocks had to be assumed for the Ibbenbüren area in order to obtain a perfect visual fit. Lithologies were also selected based on those from the adjacent areas; as no great thicknesses of coal or salt exist (which have a great effect on thermal conductivity) and as no thick claystone sequences are involved (which bear some uncertainty with respect to compaction), the results on heat flow and thickness of eroded sedimentary rocks are regarded as well constrained.

Alternative models were tested by using (1) the assumption of very deep burial for the Ibbenbüren area (8,000 m, Baldschuhn and Kockel 1999) and (2) the assumption of very high Late Cretaceous heat flows (155 mW/m^2, Buntebarth 1985). In the first case, a very low heat flow of 40 mW/m^2 had to be applied to gain some match (Fig. 6c). However, even with this unrealistic scenario, the shape of the calculated trend line differs very much from that of the trend line for measured vitrinite reflectance data. Furthermore, the influence of a possible thermal (magmatic) event on the maturity pattern during the early Late Cretaceous was investigated by increasing heat flow values up to 155 mW/m^2 (Buntebarth 1985) during that time. If this high heat flow is combined with the assumption of an eroded thickness of 4,000 m, calculated vitrinite reflectance values of 4% for surface sediments result, increasing extremely with depth. These values are far too high. In order to obtain a fit for the uppermost sedimentary rocks, a much lower rate of erosion of 2,217 m was applied (Fig. 6d). In this scenario, a fit between measured and calculated vitrinite reflectance data could be achieved for the uppermost sedimentary rocks only, but the reflectance gradient is completely different from that displayed by the real maturity data. Accordingly, both

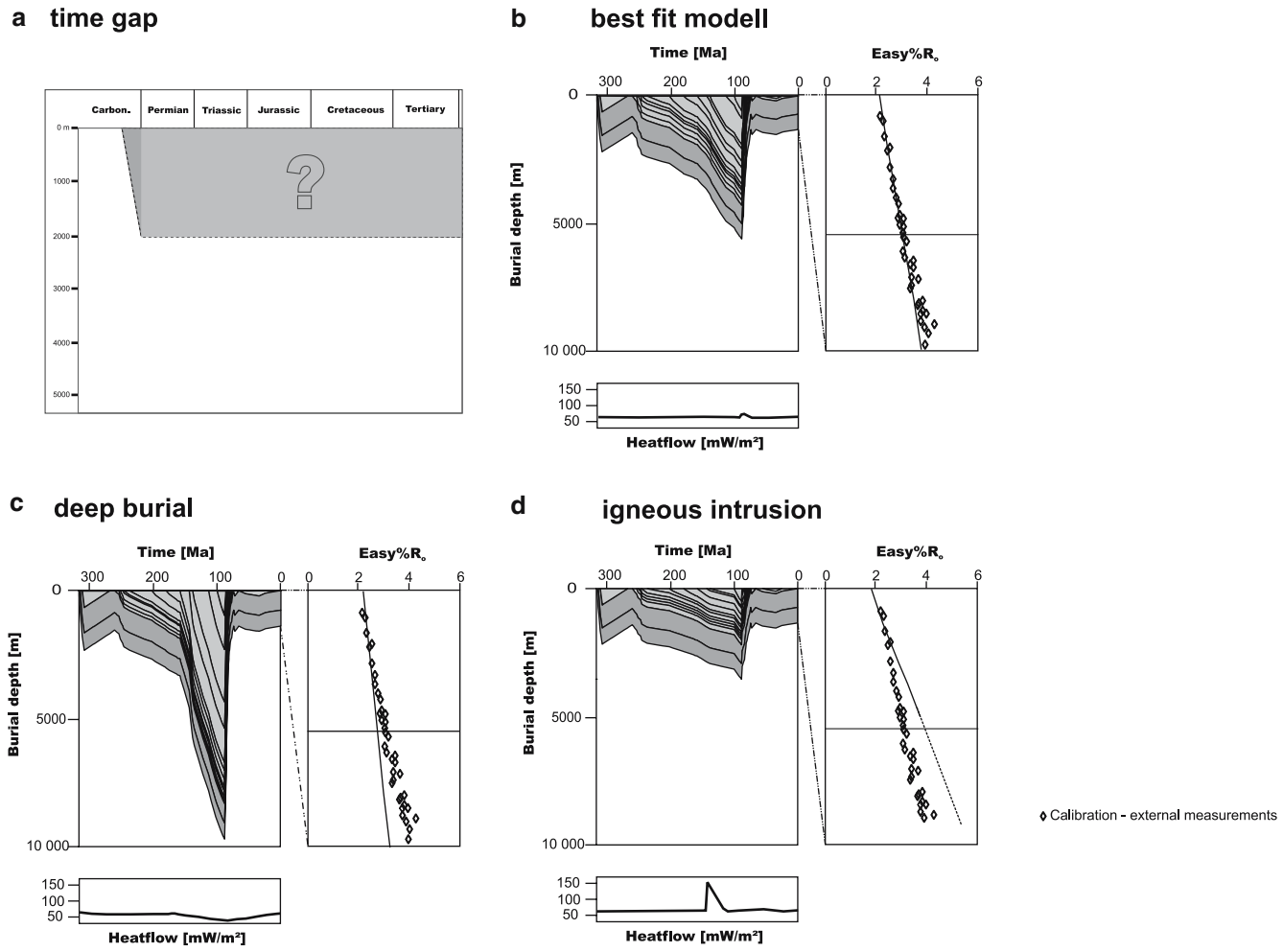

Fig. 6 Results of numerical modelling for the Ibbenbüren area near the southern border of the LSB. **a** Shows the time gap in the sedimentary sequence. **b** Shows the best-fit model with a former, now-eroded overburden of 4,407 m and a heat flow of 70 mW/m^2. In (**c**) the theory of an additional overburden of 8,000 m after Baldschuhn and Kockel (1999) is tested and (**d**) depicts the assumption of an igneous intrusion (after Buntebarth 1985) with a heat flow of 155 mW/m^2 and additional overburden of 2,217 m

the high heat flow and the extreme burial hypotheses have to be discarded.

Thermal modelling: the Bramsche area (central LSB)

Well G serves as an example for the thermal history in the central part of the maturity anomaly of the LSB (Fig. 2). This well penetrated a succession of Upper Jurassic to Carboniferous (Westphalian D) sedimentary rocks and reached a final depth of 3,644 m. Vitrinite reflectance values measured on organic-matter-bearing shales increase with depth from 2.6 to 4.6%VRr (Table 1, Fig. 2). These values imply that the organic material reached the meta-anthracitic stage and experienced temperatures exceeding 250°C. At such high maturity levels, it becomes extremely difficult to distinguish primary and secondary organic particles such as vitrinite, inertinite, and solid bitumen. Moreover, in Well G vitrinite reflectance is also influenced by dispersed hydrothermal microveins. In this study, thermally altered vitrinites were found within hydrothermal quartz showing reflectance values of more than 13%. Thus, the hydrothermal alteration took place at temperatures much higher than 480°C and might have also influenced the reflectance pattern in the vicinity of the veins. Such circumstances cause a larger scatter of vitrinite reflectance at great depths; for example,Teichmüller et al. (1979) measured vitrinite reflectance values of 5.1–5.8%VRr for the Upper Carboniferous which are higher than those determined by other authors. Clearly, the quality of maturity data for Well G is not as excellent as in the case of the Ibbenbüren area. However, the effect on the calibrated numerical models, for example, on calculated eroded thickness and heat flow during times of maximum temperatures is not very large.

Cretaceous sedimentary rocks are missing in the central part of the LSB around Well G (Fig. 7a), but are preserved in more marginal parts of the LSB. Cumulative thickness of preserved Cretaceous sedimentary

rocks in the vicinity of the area is about 3,300 m. This value gives a first indication on eroded sediment thickness, but may be misleading, because the layer thickness can increase significantly towards the basin centre (e.g. Petmecky et al. 1999). A good fit between measured and calculated reflectance was achieved assuming a heat flow of 63 mW/m^2 during maximum burial. Furthermore, the now-eroded overburden has a thickness of 3,985 m (Cretaceous: 3,825 m) according to the best-fit model (Fig. 7b). This eroded thickness was attributed to Tithonian to Coniacian sedimentary rocks (see Fig. 7a) and is about 1,655 m higher than the thickness of the same stratigraphic interval calculated for adjacent areas (2,330 m in the Ibbenbüren area). Accordingly, a maximum heat flow/minimum erosion scenario and a minimum heat flow/maximum erosion scenario were created. According to these alternative models, a heat flow of at least 60 mW/m^2 and at most 65 mW/m^2 can be assumed to have occurred during the time of maximum temperature and maximum burial, that is, during the early Late Cretaceous. These values are in any case far lower than heat flows resulting from a large igneous intrusion (100–200 mW/m^2; Poelchau et al. 1997). Furthermore, the minimum thickness of eroded Cretaceous sedimentary rocks is 3,725 m and the maximum thickness is 3,925 m (including the Münder Marl formation). These values indicate that, similar to the southern margin of the LSB further east, huge sedimentation followed by erosion affected the central/southern LSB. Additionally, alternative models with (1) a former overburden thickness of only 2,960 m (according to Klassen 1984, Fig. 7c) and (2) an intrusive model with heat flows of 155 mW/m^2 (Fig. 7d) during the early Late Cretaceous were tested. In both cases, a fit between measured and calculated vitrinite reflectance data could be achieved for the uppermost sedimentary rocks only, but not for the deeper strata because the calculated vitrinite reflectance–depth gradient differs significantly from the measured gradient.

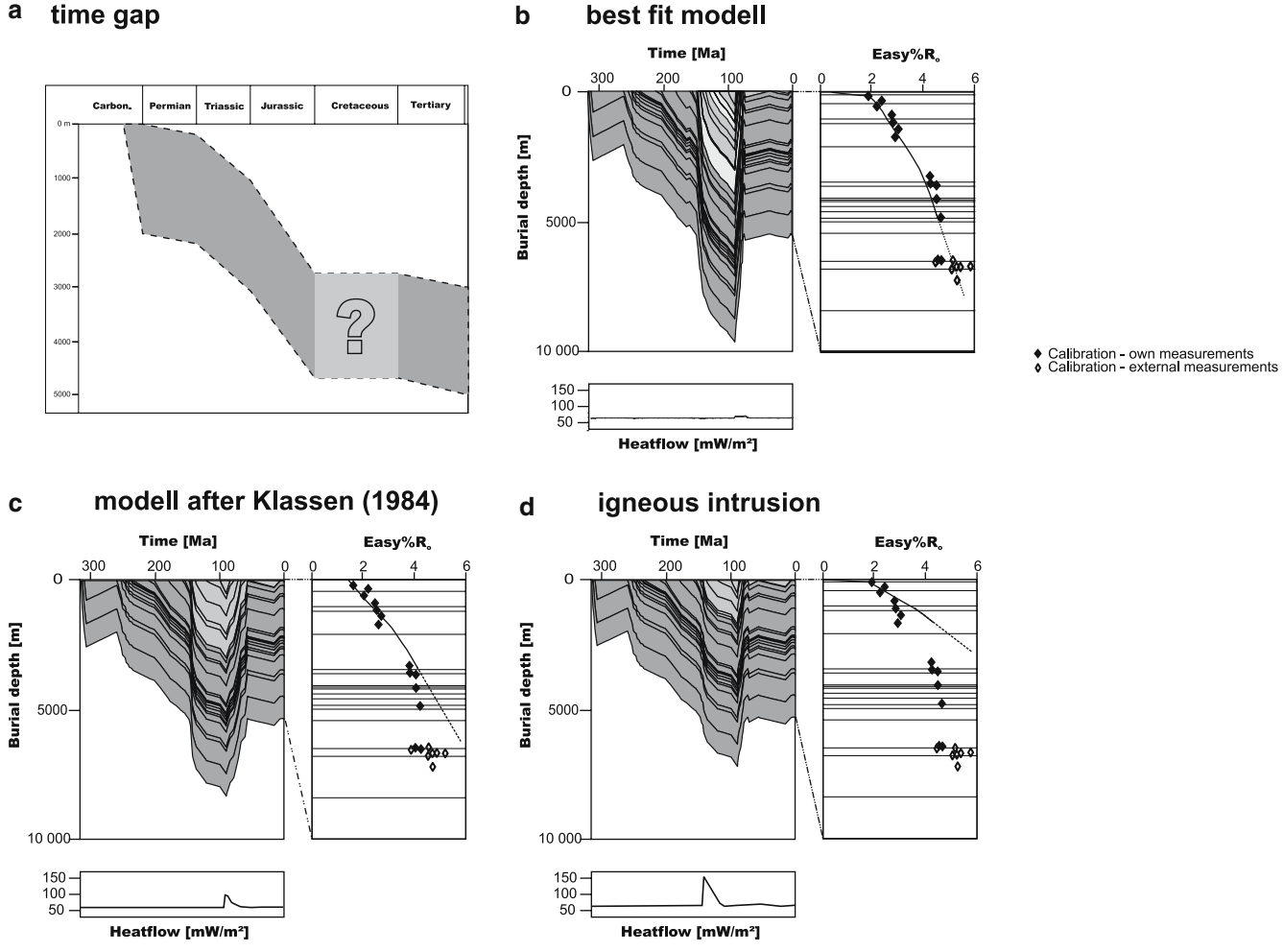

Fig. 7 Results of numerical modelling for the Bramsche area in the centre of the LSB. **a** Time gap in the sedimentary sequence between Late Jurassic and Tertiary for this area. **b** Best-fit model for Well G with a heat flow of 63 mW/m^2 and a former overburden of 3,985 m. **c** No fit achieved with a cumulative former overburden thickness of only 2,250 m (after Klassen 1984). **d** No fit achieved with assumptions of high heat flow due to an igneous intrusion (heat flow of 155 mW/m^2)

Thermal modelling: the northern LSB margin

In the northern part of the LSB, the missing stratigraphic section is much smaller than in the central and southern part; for example, in Well D only the Valanginian to Eocene section is missing (Fig. 8a). Good calibration data are available for this well from the Hauterivian to the Carboniferous interval allowing to establish a valid maturity trend (Fig. 8b). This trend can be modelled with a heat flow of 60 mW/m^2 during maximum temperature/maximum burial and a thickness of eroded Cretaceous sedimentary rocks of only 1,275 m. These results indicate that only the central part of the LSB was a deep depocentre during Early Cretaceous and early Late Cretaceous times, whereas the southern and northern margins were areas of moderate subsidence.

Thermal modelling: synthesis of results, and general discussion

The modelling technique described above was applied to a total of six wells and two pseudowells in the study area. The concept of pseudowells is described in detail in Noeth et al. (2001). Results are summarized in Figs. 9 and 10 as well as Table 4.

In the best-fit models calibrated by vitrinite reflectance data, palaeo-heat flows of 60–70 mW/m^2 had to be assumed for the time of maximum burial and temperature, that is, the early Late Cretaceous. This combination exceeds and overwhelmed the thermal effect of the volcanic event during Rotliegend times. After Bodri and Bodri (1985), the heat flow data for the time of maximum burial imply a crustal thickness of 31–35.5 km. For some areas such as the Piesberg, only maturity information from surface outcrops was available, but no vitrinite reflectance–depth profile. In this case, the heat flow results from the closest well nearby was used as input data in the modelling; in these cases, only the eroded thickness is a modelling result and not the heat flow. It should also be noted that in general only heat flow during time of maximum temperature (Late Cretaceous) may be derived from modelling, because vitrinite reflectance is mainly affected by the maximum temperature reached during burial. Accordingly, periods during which temperatures were by more than 20–30°C below the maximum temperature did hardly affect vitrinite reflectance values (Burnham and Sweeney 1989; Barker and Pawlewicz 1994). Therefore, considering only vitrinite data, there are only few constraints on heat flow evolution during pre-Cretaceous times, other than the exclusion of exceptionally high vitrinite reflectance modifying 'thermal spikes'. For the latest Cretaceous and Tertiary, it seems to be reasonable to assume heat flows of about 60–70 mW/m^2 which are similar to both the modelled Cretaceous heat flows and the present-day heat flows (Haenel 1980).

The resulting heat flows during maximum burial and temperature in the Cretaceous show a slightly increasing trend towards the south and a regional maximum in the area of Ibbenbüren and Osnabrück. Increasing heat flows are associated with periods of lithospheric stretching and thinning as well as asthenospheric rise (Yalcin et al. 1997). Correlation of heat flow variation and crustal thickness would allow to suggest a crustal-thinning event from the northern margin (35.5 km) towards the southern basin (31 km). After Allen and Allen (1990), this is in accordance with an active syn-rift event in an extensional basin. The calculated average temperature gradient for the upper 5–8 km of the crust during time of maximum burial varied between 43°C/km on the margins and 47°C/km in the centre of the basin. Thus, the palaeotemperatures at the top of the Carboniferous during maximum burial varied between 207°C (southern margin) and 224°C (northern margin), reaching up to 375°C in the centre of the study area.

All modelled Cretaceous heat flow values are in the range of normal continental heat flows and also in the

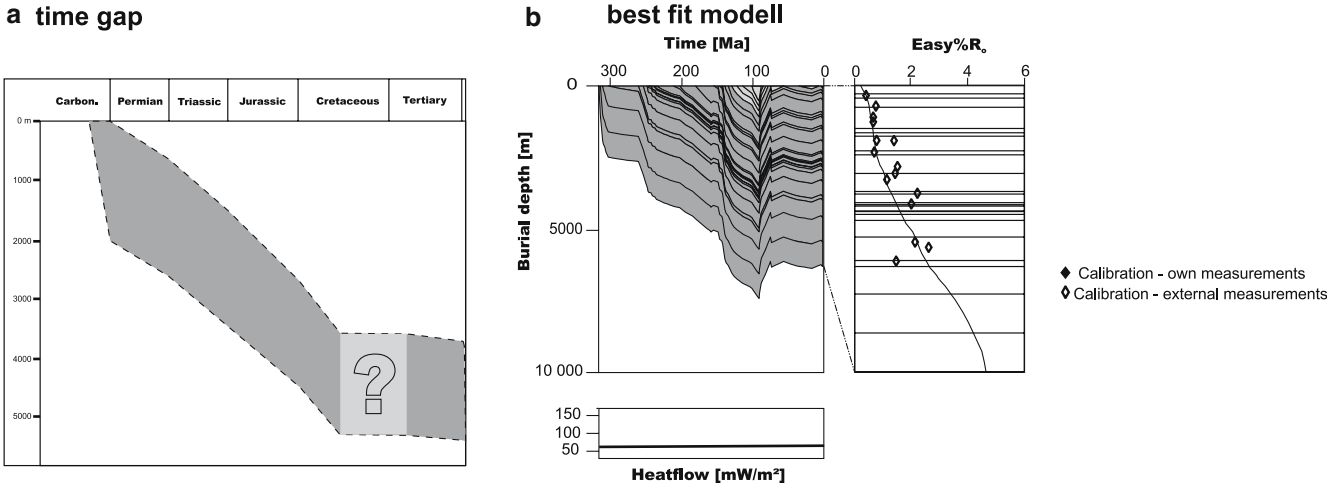

Fig. 8 Result of numerical modelling for the northern part of the LSB. **a** Time gap between the Valanginian and Tertiary. **b** Best-fit model with a former overburden of 1,275 m and a heat flow of 60 mW/m^2

Table 4 Modelled, now-eroded, former overburden and calculated heat flow values for wells in the LSB

Well	D	G	H pseudowell	I	K	L	M pseudowell	N
Heat flow [mW/m^2]	60	63	65	60	60	70	70	70
Former overburden thickness in [m] (in parentheses the preserved 'thickness)								
Total:	1,275	3,985	5,150	5,905	5,525	4,407	7,266	4,417
kro	525	525	525	525	525	600	525	600
kru	750 (298)	1,650	1,650	1,650	1,650	1,360	1,950	1,410
Berriasian		1,650	2,050	1,700	1,650	170	1,850	750
jo		160 (590)	925 (75)	750	750	500	800	500
jm				450	450	260	490	260
ju				750	500 (248)	440	625	440
k				80 (230)		225	300	225
m						152	150	152
s						500	400	80 (377)
z						200	176	

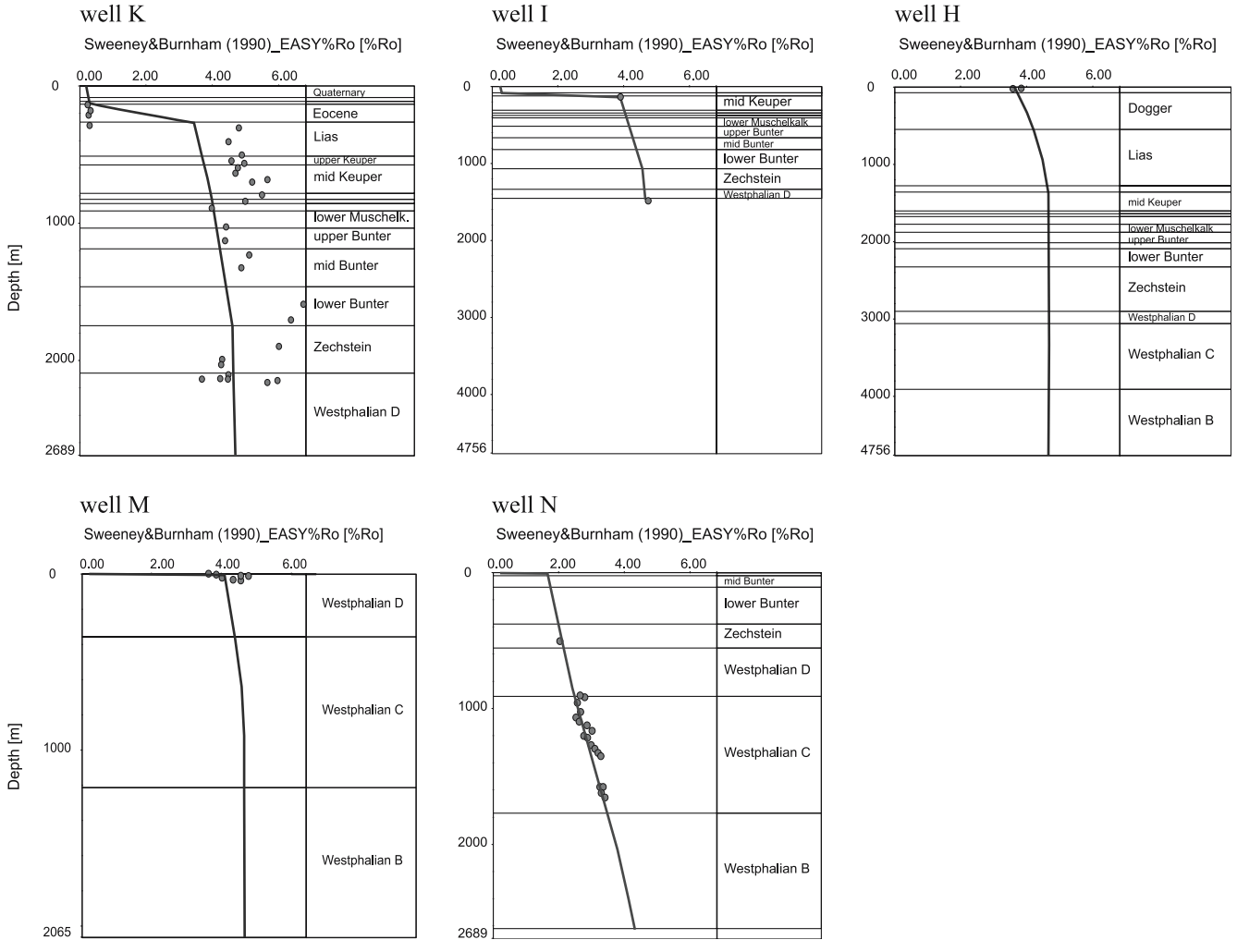

Fig. 9 Vitrinite reflectance calibration for different wells within the LSB with the algorithm of Sweeney and Burnham (1990)

range of heat flows currently present in the study area. None of the modelling results is in accordance with coalification being due to a magmatic intrusion. This conclusion does, however, not exclude the presence of a deep-seated intrusion. Such an intrusion would not necessarily have had any influence on the maturation pattern. For example, it could be of Permian age, for which large-scale extension in the Central European Basin system is postulated; in this case, it would have affected the deep-lying Pre-Permian rocks only, but the

effect on the uppermost Carboniferous units, lying close to Earth surface at that time, would have been small. This small additional maturation would have been later overprinted by deep burial during the Cretaceous. In summary, the present-day coalification pattern with anthracitic organic matter outcropping at the surface may well be explained by deep burial of the strata.

Best-fit models also reveal a cumulative thickness of eroded sedimentary rocks between 1,275 m (northern margin) and 7,266 m (Piesberg area). The latter value is similar to that favoured by Füchtbauer and Müller (1970), who already estimated 8,000 m erosion based on compaction of Carboniferous sandstones cropping out at the Piesberg. Reconstructed rates of erosion would have been 0.53 mm/a on the top of the broadly anticlinal Nordwestfalen-Lippe-Swell and 0.091 mm/a on its northern margin [for comparison: Eastern Himalaya: erosion of 2.9 mm/a; Western Himalaya: 1 mm/a (Galy and France-Lanord 2000)]. These erosion rates are based on the assumption of continuous erosion at constant rates between the onset of uplift (Coniacian; about 89 mya) and the end of Santonian times. In reality, erosion rates were certainly variable, reaching much higher values over short times. The numbers above do, however, demonstrate that no exceptionally high erosion rates have to be assumed for this area. Accommodation space for the voluminous eroded sediments was available towards the south in the Münsterland area and towards the north in the area of the Pompeckj Swell both of which were subsiding during Late Cretaceous times.

In order to construct burial history curves, information on eroded thickness for individual stratigraphic successions was deduced from data on the thickness of geological formations still preserved in other wells within the LSB or in outcrop areas at its southern margin. The thickness of eroded Cretaceous units was calculated from the difference between modelled cumulative eroded thickness and the thickness of all eroded pre-Cretaceous units (see Table 4). This calculation results in up to 4,225 m of eroded Cretaceous sedimentary rocks (including the upper Münder Marl; see Table 4) and up to 5,150 m of eroded Cretaceous plus Upper Jurassic rocks. The highest values were deduced for the Gehn area near Bramsche.

For the Late Jurassic and Cretaceous, a very high thickness results in the central LSB, for example, at Well G or in the Piesberg area. A much lower thickness is calculated for these stratigraphic units at the northern and southern margin (Wells D, L, and N), whereas the adjacent Münsterland Swell and Pompeckj Swell were uplifted during this period. The differences of eroded thicknesses represent variable synsedimentary subsidence within the LSB during late Jurassic and early Cretaceous times. Two different scenarios can explain the subsidence pattern.

The first simpler possibility is a classical, roughly E–W trending extensional basin, with the Pompeckj Swell and the Münsterland Swell acting as graben shoulders of the LSB, which were uplifted by at least several hundred metres during Late Jurassic/earliest Cretaceous times. In this case, secondary halfgraben and graben systems should follow the trend of the basin. The same can be imagined for the general trend of the isolines of coalification, as may be seen in the right (eastern) part of Fig. 2, if a secondary structure was formed homogeneously within a short time over its whole length. However, this is not necessarily the case always. The main gradient of coalification (within one layer) should generally be oriented perpendicularly to the basin direction and should display sudden changes near the boundary faults of secondary grabens or half grabens, but only small changes along strike. Resulting differences in maturity can be explained as well by a normal as by an asymmetric basin fill. The main boundary faults of the basin in this configuration, however, do not trend

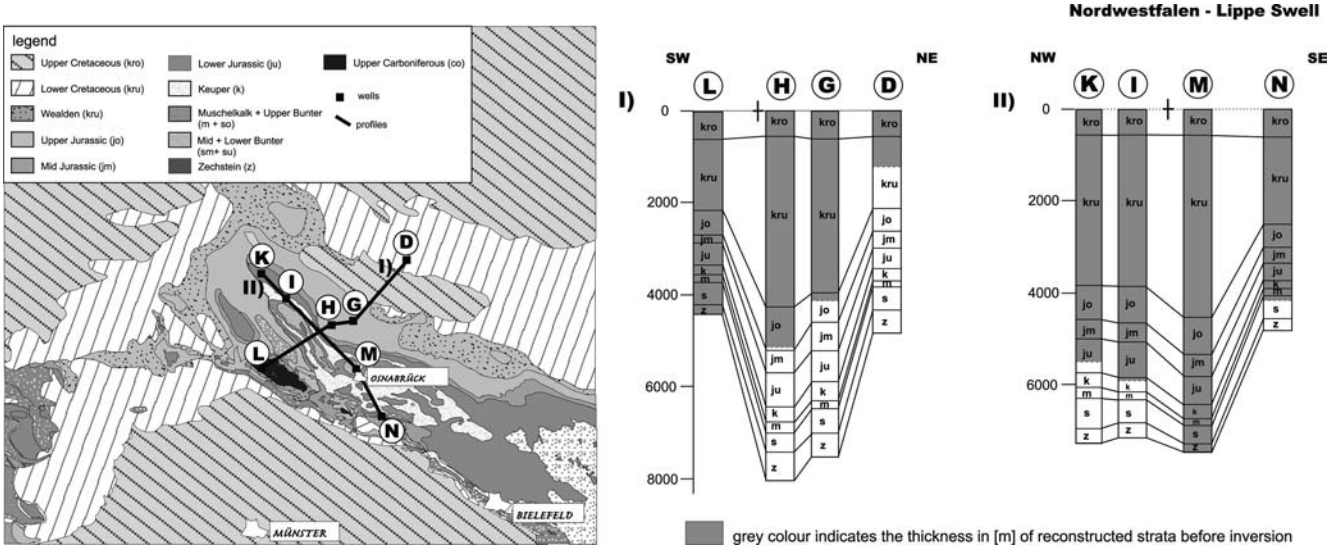

Fig. 10 Geological map and modelling results on eroded thickness along two profiles through the LSB

E–W, but WNW–ESE and display in some places an en-echelon pattern, indicating the involvement of a shear component in the formation of the basin. Therefore, a second, but more complicated model must be considered as well.

The alternative possibility is a pull-apart basin created due to horizontal movements between Pompeckj Swell/LSB and LSB/Münsterland Swell. In such a context, the fracture pattern may include master faults with associated syn- and antithetic strike-slip faults as well as additional normal faults or thrusts in specific orientations, resulting in a strongly differentiated and asynchronous basin fill (see, e.g. the Variscan Saar–Nahe basin, Hertle and Littke 2000). Variations in synsedimentary subsidence are observed especially near the tips of strike-slip faults, where small lateral offsets may lead to considerable vertical displacements (Drozdzewski and Wrede 1994; Voigt et al. 2002). The resulting thickness and maturation pattern does no longer reflect the regional distribution of source areas and the general basin configuration, but instead the geometry of commonly rhomboid fault-bounded troughs and blocks. Such a pattern seems to be indicated by the isolines of coalification in the left (western) part of Fig. 2.

More detailed analysis of the basin fill and the fault inventory with respect to the evolution of stress will be carried out in the framework of a current research programme (DFG SPP 1135) and should help to discriminate and explain the patterns described above in detail. At present, the controversial debate is going on with respect to the role of horizontal movements in the CEBS. Furthermore, salt movements might have modified the subsidence pattern dramatically. At present, little Permian salt is present in the LSB, whereas it is known in great thickness in the area of the Pompeckj Swell, forming large salt domes and salt walls. As salt can flow over large horizontal distances (Diegel et al. 1995), the possibility cannot be excluded that much more salt was initially present in the LSB which escaped northwards during Late Jurassic/Cretaceous times, leading to an enforced subsidence in the LSB and a contemporaneous uplift of the Pompeckj Swell.

Uncertainties in modelling results

In numerical modelling of complex systems, analysis of uncertainties is necessary in order to evaluate the range of possible models which would still fit the observations. Important uncertainties in basin modelling studies are related to petrophysical properties, mode of heat transfer, calibration data, and/or the algorithm of calculation for calibration data.

With respect to petrophysical properties, the thermal properties heat conductivity and heat capacity are treated here. Others, such as porosity evolution and compaction or permeability distribution as related to fluid flow are beyond the scope of this study. Thermal rock properties were not directly measured for this study, but calculated based on lithology (see above). As there is little salt and coal in the Mesozoic sedimentary sequence, the greatest uncertainty is probably the heat conductivity of sandstones. The latter differ in heat conductivity due to their quartz content, this mineral having a much higher heat conductivity than feldspars and clay minerals (Yalcin et al. 1997). The default values used for conductivity of sandstones in the PetroMod software are according to experience (e.g. Hertle and Littke 2000) either correct or lower than the real values, that is, the default values are at the lower end of the probable variation. The effect of high sandstone conductivities on modelling results is tested in the following: if sandstone conductivity would be 30% higher than the one used in this simulation and if it is assumed that these sandstones of higher conductivity represent 20% of the sedimentary sequence, a heat conductivity for the entire sequence would result which is 6% higher than the one used in the best-fit models. As $\mathrm{grad}T = Q/K$ with Q being the heat flow and K being the heat conductivity, such a misfit would lead to calculated heat flows during maximum burial which are slightly (6%) lower than those given above (Table 4). This difference would not influence the conclusions in this paper.

Also, an alternative mode of heat transfer should not affect the presented conclusions. In principle, water flow (convection) can disturb the temperature field in sedimentary basins significantly. However, to be efficient such convective processes need highly permeable pathways; the generally clay-rich Lower Cretaceous units do not seem to be suitable for this (Table 2). Furthermore, there is ample evidence that the entire LSB was strongly heated during the Cretaceous and not only those units adjacent to permeable fractures. Another option would be the assumption of high radiogenic heat production within the LSB, leading to a rise in temperature. This factor is taken into account by the software; any additional radioactive heating effect would demand more than the average percentages of radioactive elements. No evidence for this is available. If there had been a greater radiogenic heat production, slightly lower heat flows than those presented in Table. 2 and 4 would result. This modification would not influence the conclusions presented here.

The third uncertainty is the quality of calibration data used in the modelling. Here, excellent calibration data were available for some areas (e.g. Ibbenbüren, see Fig. 6) and also for other wells. High-quality data could be obtained from literature and own measurements. Even if some of the data would be false, an excellent data set would remain unchallenged.

The greatest uncertainty seems to be lying in the algorithm to calculate vitrinite reflectance. Here, the equations of Sweeney and Burnham (1990) were used which are at present regarded as state-of-the-art (Waples et al. 1992; Yalcin et al. 1997). However, this method is not well tested for the very high levels of coalification which are found in the central and southern parts of the

LSB. In order to address this concern the algorithms of Lopatin (1971, TTI) and Yamaji (1986) were tested and provided additional evidence for deep burial rather than magmatic intrusion. The lowest overburden (eroded Cretaceous thickness) resulted from the method of Barker and Pawlewicz (1994). Their equation, applied to the data of well G, results in only 3,685 m of overburden rather than 3,985 m in the best-fit model (Fig. 11), assuming an average temperature gradient in the uppermost crust at the time of maximum temperature (early Late Cretaceous) of ~43°C/km. Although the best-fit model presented here is clearly preferred, even the results reached by applying the latter approach would not affect the general conclusions.

Conclusions

Numerical simulations of burial history for various deep wells and two outcrop areas at the basin margin as well as detailed coalification studies in the LSB revealed the following:

- Basin inversion caused uplift and erosion of Mesozoic sedimentary rocks. Eroded thicknesses ranged from approximately 1,275 to approximately 7,266 m with a southward increasing trend. Erosion occurred during Coniacian or post-Coniacian times. Reconstructed rates of erosion were 0.53 mm/a on the top of the broadly anticlinal Nordwestfalen-Lippe Swell and 0.091 mm/a on the northern margin.
- Heat flow values during maximum burial range from 60 to 70 mW/m^2. These values imply a concurrent crustal thickness of 31–35.5 km. The crustal heat flow increases from the northern basin margin towards the Nordwestfalen-Lippe Swell.
- Coalification is pre-kinematic with respect to the inversion and reflects the former accumulation settings. The generally observed NW–SE striking maturity pattern of the Kimmeridgian strata can be explained by different sedimentation patterns. This is due to the fact that there are still not enough data to characterize the tectonic regime clearly.
- A thermal influence of a magmatic intrusion in the study area is not evident from the modelling approach. Thus, the theory of an igneous Cretaceous intrusion as cause for the coalification pattern appears not to be supported by the results of this modelling study. Fission track analysis on apatites and zircons is currently being performed and will provide additional information on the maximum temperature and the cooling and uplift history.

Acknowledgements This work was financially supported by the Deutsche Forschungsgemeinschaft (DFG grant no. Li 618/12) in the framework of the priority programme 1135 'Dynamics of sedimentary basins under varying stress regimes: the example of the Central European Basin System'.

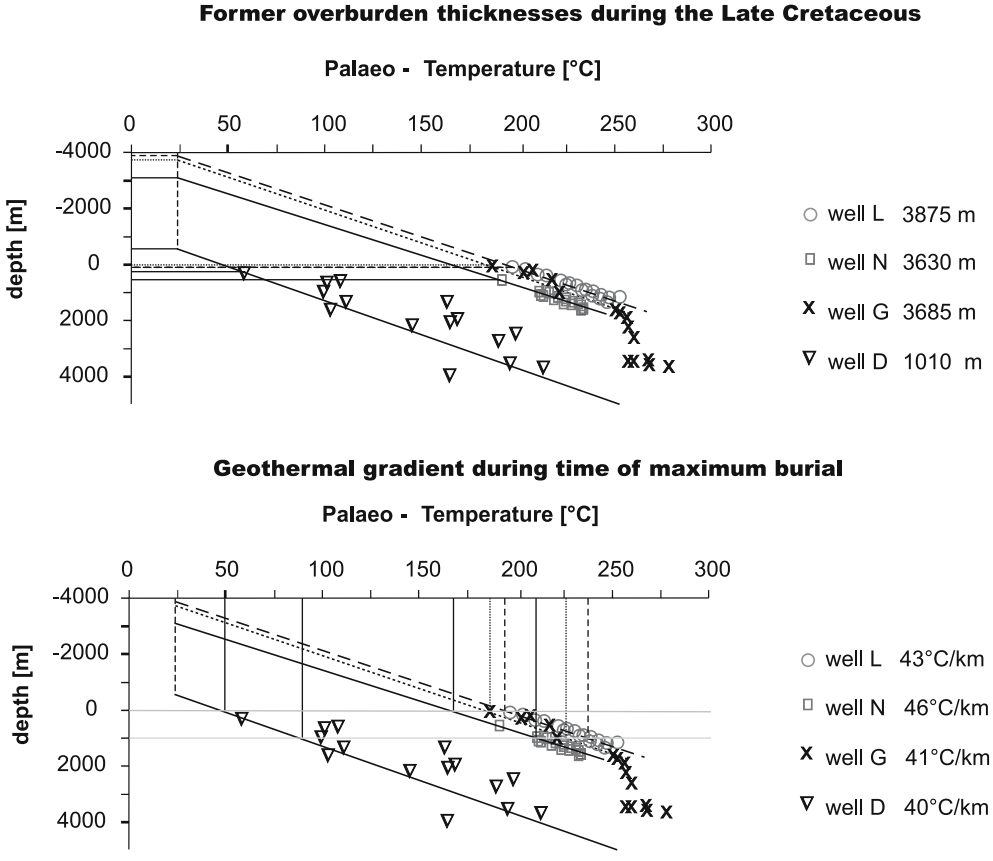

Fig. 11 Estimation of former overburden thicknesses and average geothermal gradients at the time of maximal burial for different wells according to the algorithm of Barker and Pawlewicz (1994)

References

Allen PA, Allen JR (1990) Basin analysis: principles and applications. Blackwell, Oxford, p 451

Bachmann GH, Grosse S (1989) Struktur und Entstehung des Norddeutschen Beckens—Geologische und geophysikalische Interpretation einer verbesserten Bouguer-Schwerekarte. Das Norddeutsche Becken, vol 2. Nds Akad Geowiss Veröff, Hannover, pp 23–47

Baldschuhn R, Kockel F (1999) Das Osning-Lineament am Südrand des Niedersachsen-Beckens. Z Dtsch Geol Ges 150(4):673–695

Baldschuhn R, Best G, Kockel F (1991) Inversion tectonics in the north–west German Basin. In: Spencer AM (ed) Generation, accumulation and production of Europe's hydrocarbons. EAPG, Special Publication, pp 149–159

Baldschuhn R, Binot F, Fleig S, Kockel F (2001) Geotektonischer Atlas von Nordwest-Deutschland und dem deutschen Nordsee-Sektor: Strukturen, Strukturentwicklung, Paläogeographie. Geol Jb A 153:3–95 (3 CD-ROM)

Barker CE, Pawlewicz MJ (1994) Calculation of vitrinite reflectance from thermal histories and peak temperatures. A comparison of methods. In: Dow PKMWG (ed) Vitrinite reflectance as a maturity parameter: applications and limitations. ACS Symposium Series, pp 216–229

Bartenstein R, Teichmüller R, Teichmüller M (1971) Die Umwandlung der organischen Substanz im Dach des Bramscher Massivs. Fortschr Geol Rheinl u Westf 18:501–538

Betz D, Führer F, Greiner G, Plein E (1987) Evolution of the Lower Saxony Basin. Compressional intra-plate deformations in the Alpine Foreland. Tectonophysics 137:127–170

Bodri L, Bodri B (1985) On the correlation between heat flow and crustal thickness. Tectonophysics 120:69–81

Breyer F (1971) Geophysikalische und geologische Beiträge zur oberflächennahen Tektonik im Dach des Bramscher Massivs. Fortschr Geol Rheinl u Westf 18:353–386

Brink HJ (2002) Die Anomalie von Bramsche—Wieder eine offene Frage. Erdöl Erdgas Kohle 118(1):18–22

Büker C, Littke R, Welte DH (1995) 2d-Modelling of the thermal evolution of carboniferous and devonian rocks of the Eastern Ruhr Basin and Northern Rhenish Massif, Germany. Z Dtsch Geol Ges 146(2):321–339

Buntebarth G (1985) Das Temperaturgefälle im Dach des Bramscher Massivs aufgrund von Inkohlungsuntersuchungen im Karbon von Ibbenbüren. Fortschr Geol Rheinl u Westf 33:255–264

Buntebarth G, Teichmüller R (1979) Zur Ermittlung der Paläotemperaturen im Dach des Bramscher Intrusivs aufgrund von Inkohlungsdaten. Fortschr Geol Rheinl u Westf 27:171–182

Burnham AK, Sweeney JJ (1989) A chemical kinetic model of vitrinite reflectance maturation. Geochim Cosmochim Acta 53:2649–2657

Diegel FA, Karlo JF, Schuster DC, Shoup RD, Tauvers PR (1995) Cenozoic structural evolution and tectono-stratigraphic framework of the northern Gulf Coast continental margin, vol 65. In: Jackson MPA, Roberts DG, Snelson S (eds) Salt tectonics; a global perspective. AAPG Mem, pp 109–151

Drozdzewski G (1988) Die Wurzel der Osning-Überschiebung und der Mechanismus herzynischer Inversionsbewegungen in Mitteleuropa. Geol Rundschau 77(1):127–141

Drozdzewski G (2003) Geologische Entwicklung und tektonischer Bau. In: Geologischer Dienst NRW (ed) Geologie im Weser- und Osnabrücker Bergland. Krefeld, pp 16–30

Drozdzewski G, Wrede V (1994) Faltung und Bruchtektonik—Analyse der Tektonik im Subvariscikum. Fortschr Geol Rheinl u Westf 38:7–187

Flotow AV, Berroth A, Schmehl H (1931) Relative Bestimmungen der Schwerkraft auf 115 Stationen in Norddeutschland. Veröff preuß geodät Inst 106:1–88

Füchtbauer H, Müller G (1970) Sedimente und Sedimentgesteine. Sediment-Petrologie T II. Schweizerbart, Stuttgart, p 726

Galy A, France-Lanord C (2000) Higher erosion rates in the Himalaya: geochemical constraints on Riverine Fluxes. J Conf Abstr 5(2):423

Geologischer Dienst NRW (2003) Geologie im Weser- und Osnabrücker Bergland. Krefeld, p 219

German Stratigraphic Commission (2002) A geological time scale 2002. In: G S Commission (ed) Stratigraphic Table of Germany 2002, Potsdam

Giebeler-Degro M (1986) Zur Tiefenerkundung des Niedersächsischen Tektogens durch dreidimensionale Simulationsrechnung. Unpublished Thesis, TU Clausthal, p 202

Gramann F, Heunisch C, Klassen H, Kockel F, Dulce G, Harms F-J, Katschorek T, Mönnig E, Schudack M, Schudack U, Thies D, Weiss M (1997) Das Niedersächsische Oberjura-Becken-Ergebnisse interdisziplinärer Zusammenarbeit. Z Dtsch Geol Ges 148/2:165–236

Günther K, Drozdzewski G, Hiss M (1998) Neue Erkenntnisse zum geologischen Bau des "Kleinen Berges" zwischen Bad Laer und Bad Rothenfelde (südwestliches Niedersachsen) aufgrund der Ergebnisse der Tiefbohrung 'Bad Laer Z 1'(1993). Mitt Geol Inst Univ Hannnover 38:87–113

Haenel R (1980) Atlas of subsurface temperatures in the European community. Commission European Community, 43 maps Brussels

Hahn A, Kind EG (1971) Eine Interpretation der magnetischen Anomalie von Bramsche. Fortschr Geol Rheinl u Westf 18:423–428

Hertle M, Littke R (2000) Coalification pattern and thermal modelling of the Permo-Carboniferous Saar Basin (SW-Germany). Int J Coal Geol 42:273–296

Jendrzejewski L (1995) Organische Geochemie der höheren Unterkreide Nordwestdeutschlands: Ablagerungsmilieu und Zyklik. Ber Forschungszentrum Jülich 3134:1–211

Kaiser A (1930) Magnetische Vermessungen in Nordwestdeutschland, vol 2. Beitr phys Erf Erdrinde, pp 1–50

Klassen H (1984) Geologie des Osnabrücker Berglandes. Naturwiss Mus Osnabrück, p 672

Klassen H (1991) Der obere Dogger und tiefe Malm im westlichen Niedersächsischen Becken. In: Der tiefere Untergrund des nordwestdeutschen Beckens: Sedimentologie-Tektonik-Kohlenwasserstoffe. Beiträge der DGG-DGMK-Gemeinschaftstagung Braunschweig 1989, DGMK-Bericht 468:259–295

Koch J, Arnemann H (1975) Die Inkohlung in Gesteinen des Rhät und Lias im südlichen Nordwestdeutschland. Geol Jb 29:33–43

Kockel F, Wehner H, Gerling P (1994) Petroleum systems of the Lower Saxony Basin, Germany. In: Magoon LBD, Dow WG (eds) The petroleum system from source to trap. AAPG Mem, Tulsa, pp 573–586

Leischner K, Welte DH, Littke R (1993) Fluid inclusions and organic maturity parameters as calibration tools in basin modelling. In: Doré AG, Augustson JH, Hermanrud C, Stewart DJ, Sylta O (eds) Basin modelling: advances and applications. Norwegian Petrol Soc Spec Publ. Elsevier, Amsterdam, pp 161–172

Littke R, Krooß B, Idiz EF, Frielingsdorf J (1995) Molecular nitrogen in natural gas accumulations: generation from sedimentary organic matter at high temperatures. AAPG Bull 79(3):410–430

Littke R, Cramer C, Hertle M, Karg H, Stroetmann-Heinen V, Oncken O (2000) Heat flow evolution, subsidence, and erosion in the rhenohercynican orogenic wedge of Central Europe. Geol Soc Lond Spec Publ 179:231–255

Lommerzheim A (1988) Die Genese und Migration von Kohlenwasserstoffen im Münsterländer Becken. Diss Univ Münster, p 260

Lopatin NV (1971) Temperatur und Zeit als Faktoren der Inkohlung. Akad Nauk SSSR Izv Ser Geol 3:95–106

McClay KR (1995) The geometries and kinematics of inverted fault systems: a review of analogue model studies. In: Buchanan JG, Buchanan PG (eds) Basin inversion. Geol Soc Lond, Spec Publ 88, pp 97–118

Mundry E (1971) Der Temperaturverlauf im Dach des Bramscher Massivs nach der Wärmeleitungstheorie. Fortschr Geol Rheinl u Westf 18:539–546
Mutterlose J (1992) Migration and evolution patterns of floras and faunas in marine Early Cretaceous sediments of NW Europe. Palaeogeogr Palaeoclimatol Palaeoecol 94:261–282
Mutterlose J, Bornemann A (2000) Distribution and facies patterns of the Lower Cretaceous sediments in northern Germany: a review. Cretaceous Res 21:733–759
Neunzert GH, Gaupp R, Littke R (1996) Absenkungs- und Temperaturgeschichte paläozoischer und mesozoischer Formationen im Nordwestdeutschen Becken. Z Dtsch Geol Ges 147(2):183–208
Nodop J (1971) Tiefenrefraktionsseismischer Befund im Profil Versmold-Lübbecke-Nienburg. Fortschr Geol Rheinl u Westf 18:411–422
Noeth S, Karg H, Littke R (2001) Reconstruction of Late Palaeozoic heat flows and burial histories at the Rhenohercynian–Subvariscan boundary, Germany. Int J Earth Sci (Geol Rundschau) 90:234–256
Petmecky S, Meier L, Reiser H, Littke R (1999) High thermal maturity in the Lower Saxony Basin: intrusion or deep burial? Tectonophysics 304:317–344
Plein E (1978) Rotliegend-Ablagerungen im Norddeutschen Becken. Z Dtsch Geol Ges 129(1):71–97
Poelchau HS, Baker DR, Hantschel T, Horsfield B, Wygrala B (1997) Basin simulation and the design of the conceptual basin model. In: Welte DH, Horsfield B, Baker DR (eds) Petroleum and basin evolution. Springer, Berlin Heidelberg New York, pp 3–70
Radke M, Horsfield B, Littke R, Rullkötter J (1997) Maturation effects and parameters. In: Welte DH, Horsfield B, Baker DR (eds) Petroleum and basin evolution. Springer, Berlin Heidelberg New York, pp 169–229
Scheidt G, Littke R (1989) Comparative organic petrology of interlayered sandstones, siltstones, mudstones and coals in the Upper Carboniferous Ruhr Basin, Northwest-Germany, and their thermal history and methane generation. Geol Rundschau 78(1):375–390
Schmidt A (1914) Die magnetische Vermessung I. Ordnung des Königreichs Preußen, 1898 bis 1903, nach den Beobachtungen von M Eschenhagen und J Edler. Veröff Preuß Meteorolog Inst, Berlin, pp 7 Kt
Skupin K (2003) Kreide. In: Geologischer Dienst NRW (ed) Geologie im Weser- und Osnabrücker Bergland. Krefeld, pp 65–70
Stadler G, Teichmüller M (1971) Die Umwandlung der Kohlen und die Diagenese der Ton- und Sandsteine in der Untertagebohrung 150 der Steinkohlenbergwerke Ibbenbüren. Fortschr Geol Rheinl u Westf 18:125–146
Süss MP (1996) Sedimentologie und Tektonik des Ruhr-Beckens: Sequenzstratigraphische Interpretation und Modellierung eines Vorlandbeckens der Varisciden, vol 20. Bonner Geowissensch Schriften, p 148
Sweeney JJ, Burnham AK (1990) Evaluation of a simple model of vitrinite reflectance based on chemical kinetics. AAPG Bull 74:1559–1570
Taylor GH, Teichmüller M, Davies A, Diessel CFK, Littke R, Robert P (1998) Organic petrology. Gebr Bornträger, Berlin, p 704
Teichmüller M (1963) Die Kohlenflöze der Bohrung Münsterland 1(Inkohlung, Petrographie, Verkokungsverhalten). Fortschr Geol Rheinl u Westf 1:129–178
Teichmüller M, Teichmüller R (1951) Inkohlungsfragen im Osnabrücker Raum. N Jb Geol Pal, Monatshefte 1951:69–85
Teichmüller M, Teichmüller R (1958) Inkohlungsuntersuchungen und ihre Nutzanwendung. Geol en Mijnb 20:41–66
Teichmüller M, Teichmüller R (1985) Inkohlungsgradienten in der Anthrazitfolge des Ibbenbürener Karbons. Fortschr Geol Rheinl u Westf 33:231–253
Teichmüller M, Teichmüller R, Bartenstein H (1979) Inkohlung und Erdgas in Nordwestdeutschland—Eine Inkohlungskarte der Oberfläche des Oberkarbons. Fortschr Geol Rheinl u Westf 27:137–170
Teichmüller M, Teichmüller R, Lorenz V (1983) Inkohlung und Inkohlungsgradienten im Permokarbon der Saar-Nahe-Senke. Z Dtsch Geol Ges 134:153–210
Teichmüller M, Teichmüller R, Bartenstein H (1984) Inkohlung und Erdgas—Eine neue Inkohlungskarte der Karbon-Oberfläche in Nordwest-Deutschland. Fortschr Geol Rheinl u Westf 32:11–34
Thiermann A (1970) Erläuterungen zu Blatt 3712 Tecklenburg. Geol Kt Nordrh-Westf, Erl. 3712 Tecklenburg. Krefeld, p 243
Thiermann A (1980) Erläuterungen zu Blatt 3612 Mettingen. Geol Kt Nordrh-Westf, Erl. 3612 Mettingen. Krefeld, p 200
Thyssen F, Allnoch HG, Lütkebohmert G (1971) Einige Ergebnisse geophysikalischer Arbeiten im Bereich der Bramscher Anomalie. Fortschr Geol Rheinl u Westf 18:395–410
Trusheim F (1961) Über radioaktive Leithorizonte im Buntsandstein Norddeutschlands zwischen Ems und Weser. Erdöl und Kohle 14:797–802
Voigt T, Eynatten H v, Franzke HJ, Gaupp, R (2002) Fazies, Mächtigkeiten und Herkunt der Kreidesedimente im Harzvorland—ein Schlüssel zum Verständnis der Harzhebung. In: Hüssner H, Hinderer M, Götz AE, Petschik R (eds) Schriftenreihe Dtsch Geol Ges, Kurzfassungen und Programm 'Sediment 2002' pp 211–212
Waples DW (1980) Time and temperature in petroleum formation: application of Lopatin's method to petroleum exploration. AAPG Bull 64:916–926
Waples DW, Suizu M, Kamata H (1992) The art of maturity modeling, Part 2. Alternative models and sensitivity analysis. AAPG Bull 76:47–66
Wees v J-D, Stephenson RA, Ziegler PA, Bayer U, McCann T, Dadlez R, Gaupp R, Narkiewicz M, Bitzer F, Scheck M (2000) On the origin of the Southern Permian Basin, Central Europe. Mar Petrol Geol 17:43–59
Welte DH, Yalcin MN (1988) Basin modelling—a new comprehensive method in petroleum geology. Org Geochem 13(1–3):141–151
Welte DH, Yükler MA (1981) Petroleum origin and accumulation in basin evolution. AAPG Bull 65:1387–1396
Wygrala B (1989) Integrated study of an oil field in the southern Po-basin, Northern Italy. Diss Univ Köln, Ber Forschungszentrum Jülich, 2313, p 217
Yalcin NM, Littke R, Sachsenhofer RF (1997) Thermal histories of sedimentary basins. In: Welte DH, Horsfield B, Baker DR (eds) Petroleum and basin evolution. Springer, Berlin Heidelberg New York, pp 71–167
Yamaji A (1986) Analysis of vitrinite reflectance–burial depth relations in dynamical geological settings by direct integration method. Jpn Assoc Petrol Technol 5(1/3):1–8
Ziegler PA (1982) Triassic rifts and facies patterns in Western and Central Europe. Int J Earth Sci (Geol Rundschau) 71(3):747–772
Ziegler PA (1990) Geological atlas of Western and Central Europe, 2nd edn. The Hague (Shell International), p 239